JBC RESEARCH ARTICLE

YTHDF2 protein stabilization by the deubiquitinase OTUB1 promotes prostate cancer cell proliferation *via* PRSS8 mRNA degradation

Received for publication, September 22, 2023, and in revised form, February 23, 2024 Published, Papers in Press, March 9, 2024,
https://doi.org/10.1016/j.jbc.2024.107152

Xuefeng Zhao[1], **Suli Lv**[1], **Neng Li**[1], **Qingli Zou**[1], **Lidong Sun**[1,2,*], **and Tanjing Song**[1,2,*]

From the [1]*Department of Biochemistry and Molecular Biology, School of Basic Medicine, Tongji Medical College, Huazhong University of Science and Technology, Wuhan, China;* [2]*Cell Architecture Research Institute, Huazhong University of Science and Technology, Wuhan, Hubei, China*

Reviewed by members of the JBC Editorial Board. Edited by Brian Strahl

Prostate cancer is a leading cause of cancer-related mortality in males. Dysregulation of RNA adenine N-6 methylation (m6A) contributes to cancer malignancy. m6A on mRNA may affect mRNA splicing, turnover, transportation, and translation. m6A exerts these effects, at least partly, through dedicated m6A reader proteins, including YTH domain–containing family protein 2 (YTHDF2). YTHDF2 is necessary for development while its dysregulation is seen in various cancers, including prostate cancer. However, the mechanism underlying the dysregulation and function of YTHDF2 in cancer remains elusive. Here, we find that the deubiquitinase OUT domain–containing ubiquitin aldehyde-binding protein 1 (OTUB1) increases YTHDF2 protein stability by inhibiting its ubiquitination. With *in vivo* and *in vitro* ubiquitination assays, OTUB1 is shown to block ubiquitin transfer to YTHDF2 independent of its deubiquitinase activity. Furthermore, analysis of functional transcriptomic data and m6A-sequencing data identifies PRSS8 as a potential tumor suppressor gene. OTUB1 and YTHDF2 decrease mRNA and protein levels of PRSS8, which is a trypsin-like serine protease. Mechanistically, YTHDF2 binds PRSS8 mRNA and promotes its degradation in an m6A-dependent manner. Further functional study on cellular and mouse models reveals PRSS8 is a critical downstream effector of the OTUB1–YTHDF2 axis in prostate cancer. We find in prostate cancer cells, PRSS8 decreases nuclear β-catenin level through E-cadherin, which is independent of its protease activity. Collectively, our study uncovers a key regulator of YTHDF2 protein stability and establishes a functional OTUB1–YTHDF2–PRSS8 axis in prostate cancer.

Prostate cancer presents a major challenge for male health and survival. Despite the prevailing antiandrogen therapy, the disease eventually acquires androgen independency and progresses to metastasis (1). Each year, prostate cancer causes more than 300,000 deaths worldwide (2). Uncovering novel protumor pathways in prostate cancer hold promise for unmet medical needs (3). Methylation of adenine N6 (m6A) is a widespread modification on mRNA and noncoding RNA (4). m6A has gained extensive attention in the past decade. Like the case for histone modifications, m6A also has its writers, readers, and erasers (5). m6A is mainly catalyzed by a methyltransferase complex, the "writer," which consists of the catalytic METTL3 and other subunits including METTL14 (5, 6), while METTL3 alone is catalytically incompetent. Consistently, *in vitro* and *in vivo* studies have shown that the integrity of the complex is critical for m6A installation (7, 8). Conversely, m6A can be removed by demethylase fat mass and obesity (FTO)-associated protein or ALKBH5, the “eraser” (5). m6A impacts essentially every aspect of RNA biology, including conformation, splicing, transportation, translation, and turnover of RNA (4). These pleiotropic effects can be mediated by a group of proteins recognizing the modification, including YTH domain–containing family proteins YTHDF1, YTHDF2, YTHDF3, YTHDC1, and YTHDC2 (5, 9, 10). YTH domain recognizes m6A *via* cation-pi and pi–pi interaction enabled by an aromatic cage (11–13), which is reminiscent of the recognition of methyl-lysine/arginine by royal family proteins (14). Among these YTH proteins, YTHDF2 shares similar sequence and domain arrangement with YTHDF1 and YTHDF3 (overall 55.9% identity and 77.9% similarity). YTHDF2 is ubiquitously expressed (15) and its main effect was suggested to be promoting mRNA degradation (10, 16). YTHDF2 is necessary for embryonic and somatic development (15, 17). Among the three YTHDFs, YTHDF2 knockout gives the most significant phenotype, which cannot be compensated by the other two (15). Single-allele loss of YTHDF2 in inbred mice causes developmental defects and is partially lethal, indicating dosage is a limiting factor for YTHDF2 function (17). Consistent with this notion, dysregulated expression rather than mutation of YTHDF2 is seen in various cancer types, which is mainly attributed with a protumor function albeit with controversy for liver cancer (18). In prostate cancer, YTHDF2 is overexpressed and promotes tumor growth as well as metastasis (19, 20). Accordingly, it is important for prostate cancer etiology to uncover potential mechanisms and biological consequences of YTHDF2 dysregulation. Protein ubiquitination regulates the function and turnover of a substrate

* For correspondence: Lidong Sun, LidongSun@hust.edu.cn; Tanjing Song, SongT@hust.edu.cn.

(21). In the past, ubiquitination was identified as a key mechanism modulating YTHDF2 protein level (22, 23). FBW7 (22) and SKP2 (23) were suggested to exhibit E3 ligase activity toward YTHDF2. Ubiquitination is subject to antagonizing regulation by E3 ubiquitin ligases and deubiquitinases (24). While E3 can transfer activated ubiquitin from E2 (ubiquitin-conjugating enzymes) to a substrate, deubiquitinase can remove ubiquitin through its isopeptidase activity (21). Yet, it is not known whether any deubiquitinase can regulate YTHDF2.

There are close to 100 deubiquitinases in the human genome, among which OUT domain–containing ubiquitin aldehyde-binding protein 1 (OTUB1_ belongs to the ovarian tumor domain protease (OTU) subfamily, consisting of about 16 members (25, 26). Like most other deubiquitinases, OTUB1 is a cysteine protease and contains three residues critical for catalysis, C91, H265, and D267, referred to as the "catalytic triad" (25, 27, 28). The catalytic cysteine C91 makes the nucleophilic attack at the ubiquitin-isopeptide bond, which is assisted by the other two residues (25). OTUB1 preferentially cleaves the K48-linked ubiquitin chain, which typically causes protein degradation by proteasome (27, 29). Besides the deubiquitinase/isopeptidase activity, there is yet another noncanonical mechanism by which OTUB1 inhibits protein ubiquitination. OTUB1 can bind and inhibit the function of several E2s (30, 31). This noncanonical mechanism has been shown for several different proteins, such as DEPTOR (32), MSH2 (33, 34) and P53 (35). Through either mechanism, OTUB1 regulates other proteins and has emerged as a key player in development and various diseases, including cancer (36, 37). Regarding cancer, OTUB1 has been mostly ascribed a protumor role although discrepancy was reported in some P53-WT cancer cells (35). In prostate cancer, OTUB1 was reported to promote cell proliferation and invasion (38, 39). Thereof, the protein level of cyclin E1, a marker and driver of cell proliferation, was suggested to be increased by OTUB1 (39). However, the direct effector of OTUB1 in prostate cancer remains unclear.

In this study, we find that OTUB1 binds YTHDF2 and antagonizes its ubiquitination in prostate cancer cells. Consequently, OTUB1 promotes the protein stability of YTHDF2, which in turn serves as a key mediator of OTUB1 function. We further identify protease serine S1 family member 8 (PRSS8, also known as prostasin) as a key downstream effector of the OTUB1–YTHDF2 axis. PRSS8 is a serine protease preferentially expressed in the prostate (40), which was shown to contribute to epithelial sodium channel activation and epidermis development (41, 42). Intriguingly, PRSS8 gene silencing was observed in human cancer albeit the underlying mechanisms and biological consequences remain elusive (43). In this study, we show PRSS8 protein level is decreased in prostate cancer patient samples. We find that PRSS8 inhibits prostate cancer cell proliferation independent of its protease activity. Overexpressing PRSS8 promotes epithelial morphology of prostate cancer cells with increased E-cadherin protein level and decreased nuclear β-catenin level. We reveal that YTHDF2 binds PRSS8 mRNA and promotes its degradation in an m6A-dependent manner.

Results

OTUB1 promotes YTHDF2 protein stability in prostate cancer

We set out to identify potential deubiquitinases that might regulate YTHDF2 in prostate cancer. We cross-referenced a list of known deubiquitinases and published YTHDF2 interactome datasets. YTHDF2 was identified as a potential interaction partner of OTUB1 by affinity purification coupled with mass spectrometry (44). We confirmed both exogenous and endogenous OTUB1 interacted with YTHDF2 with coimmunoprecipitation (Fig 1, *A* and *B*). We then examined whether OTUB1 regulated the YTHDF2 protein level. Knocking down OTUB1 with shRNA specifically decreased the YTHDF2 protein level in all three prostate cancer cell lines examined while YTHDF1 and YTHDF3 were not affected (Figs. 1*C* and S1*A*). This effect was abolished by rescue-expressing OTUB1, excluding it caused by the off-targeting of shRNA (Figs. 1*D* and S1*B*). Consistently, OTUB1 overexpression (OE) increased the YTHDF2 protein level (Figs. 1*E* and S1*C*). Next, we explored the mechanism by which OTUB1 regulated YTHDF2. OTUB1 knockdown (KD) did not cause change in YTHDF2 mRNA level concordant with protein level (Fig. S1*D*). With OTUB1 being a deubiquitinase, we hypothesized it might regulate YTHDF2 protein stability. We treated cells with cycloheximide (Chx) to block protein synthesis and found OTUB1-KD indeed decreased YTHDF2 protein stability (Figs. 1*F* and S1*E*). This effect was abolished by rescue-expressing OTUB1, confirming it was not due to the potential off-target effect of shRNA (Fig. 1*G*). Consistently, overexpressing OTUB1 increased YTHDF2 protein stability (Fig. 1*H*). Collectively, these results showed OTUB1 increased YTHDF2 protein stability in prostate cancer cells.

OTUB1 decreases YTHDF2 ubiquitination through a noncanonical mechanism

We next examined whether the stabilization of YTHDF2 by OTUB1 was through deubiquitination. After knocking down OTUB1, the immunoprecipitation (IP)-Western blot (WB) assay detected significantly increased ubiquitination levels of endogenous YTHDF2. The ubiquitination signal was diminished in the YTHDF2-KD cell, supporting it was specifically from YTHDF2 (Figs. 2*A* and S2*A*). To determine whether OTUB1's deubiquitinase activity was required to regulate YTHDF2 ubiquitination, YTHDF2 and ubiquitin were coexpressed with either OTUB1 WT or mutants. The C91S mutation disrupted the catalytic C91 and thus the deubiquitinase activity of OTUB1. In contrast, the alanine mutation of D88, not a "catalytic triad" residue, was used widely to abrogate the E2-inhibitory effect of OTUB1 (32, 33, 35). IP-WB showed that the C91S mutant still repressed YTHDF2 ubiquitination like its WT counterpart, disproving the effect was through direct deubiquitination (Fig. 2*B*). In contrast, the D88A mutant failed to do so, indicating the noncanonical E2-inhibiting mechanism was involved (Fig. 2*B*). Similar observation was made on DEPTOR, which was shown to be regulated by OTUB1 through noncanonical mechanism and served as a positive control here (Fig. S2*B*) (32). To further exclude OTUB1

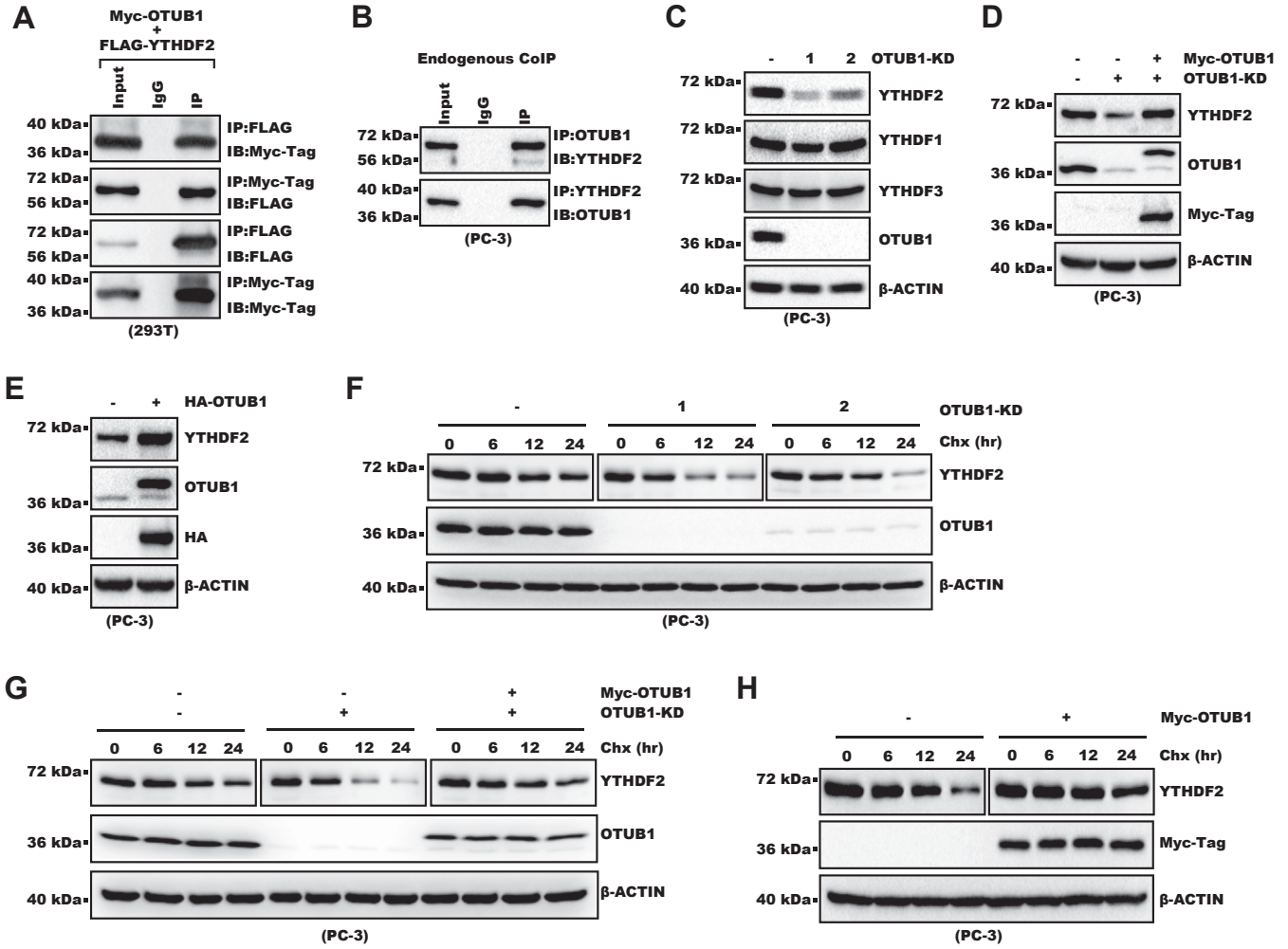

Figure 1. OTUB1 regulates YTHDF2 protein stability. *A*, 4 μg Myc-OTUB1 and FLAG-YTHDF2 plasmids were cotransfected into HEK-293T cells in a 6-cm dish. Forty eight hours later, cells were collected for Co-IP–WB analysis as indicated. "Input" denotes 1% input material for each IP. *B*, PC-3 cells were analyzed with Co-IP–WB as indicated. "Input" denotes 1% input material for each IP. *C*, OTUB1 was knocked down in PC-3 cells with shRNA. Whole-cell extracts (WCE) were then analyzed with WB. *D*, shRNA-resistant Myc-OTUB1 was introduced into OTUB1-KD PC-3 cells. WCE were then analyzed with WB. *E*, HA-OTUB1 was expressed in PC-3 cells. WCE were then analyzed with WB. *F*, control or OTUB1-KD PC-3 cells were treated with 25 μg/ml cycloheximide (Chx) for the indicated time. WCE were analyzed with WB. For YTHDF2, separate exposures for control and OTUB1-KD cells were presented to make the signals of "Chx 0 h" comparable and facilitate the comparison of protein stability. *G*, shRNA-resistant Myc-OTUB1 was rescue-expressed into OTUB1-KD cells. Cells were then treated with 25 μg/ml Chx for the indicated time. WCE were analyzed with WB. For YTHDF2, separate exposures for control, "OTUB1-KD" and "OTUB1-KD + Myc-OTUB1" cells were presented to make the signals of "Chx 0 h" comparable and facilitate comparison of protein stability. *H*, Myc-OTUB1 was expressed in PC-3 cells. Cells were then treated with 25 μg/ml Chx for different time. WCE were analyzed with WB. For YTHDF2, separate exposures for control and "Myc-OTUB1" cells were presented to make the signals of "Chx 0 h" comparable and facilitate comparison of protein stability. Co-IP, co-immunoprecipitation; HA, hemagglutinin; IP, immunoprecipitation; KD, knock down; m6A, methylation of adenine N6; OTUB1, OUT domain–containing ubiquitin aldehyde-binding protein 1; PRSS8, protease serine S1 family member 8; WB, Western blot; WCE, whole-cell extract; YTHDF2, YTH domain–containing family protein 2.

deubiquitinated YTHDF2, we performed an *in vitro* deubiquitination assay by incubating ubiquitinated YTHDF2 with recombinant OTUB1 purified from *Escherichia coli*. No significant decrease in YTHDF2 ubiquitination was detected, which further excluded direct deubiquitination (Fig. S2*C*). In contrast to DEPTOR, PD-L1 had been reported to be OTUB1's direct substrate (45). We employed it here as another control. In stark contrast to YTHDF2, PD-L1 was efficiently deubiquitinated *in vitro* by recombinant OTUB1 WT or D88A (Fig. S2*D*). This effect on PD-L1 was diminished by C91S mutation, also consistent with direct deubiquitination (Fig. S2*D*). These results all suggested OTUB1 decreased YTHDF2 ubiquitination through the noncanonical mechanism. We next directly tested whether OTUB1 inhibited ubiquitin transfer to YTHDF2 with an *in vitro* ubiquitination reaction reported previously (33). We added recombinant OTUB1 into an *in vitro* ubiquitination reaction with YTHDF2 as substrate. The result showed adding OTUB1 WT or C91S into the reaction decreased YTHDF2 ubiquitination (Fig. 2*C*). In contrast, D88A failed to do so (Fig. 2*C*). Consistently, overexpressing OTUB1-D88A *in vivo* failed to increase YTHDF2 protein level or protein stability, unlike its WT counterpart (Figs. 2, *D* and *E* and S2*E*). Altogether, these data demonstrated OTUB1 decreased YTHDF2 ubiquitination by noncanonically repressing ubiquitin transfer to YTHDF2.

YTHDF2 mediates the proproliferation effect of OTUB1

OTUB1 was reported to promote prostate cancer cell proliferation and invasion (38, 39), which we further confirmed in this

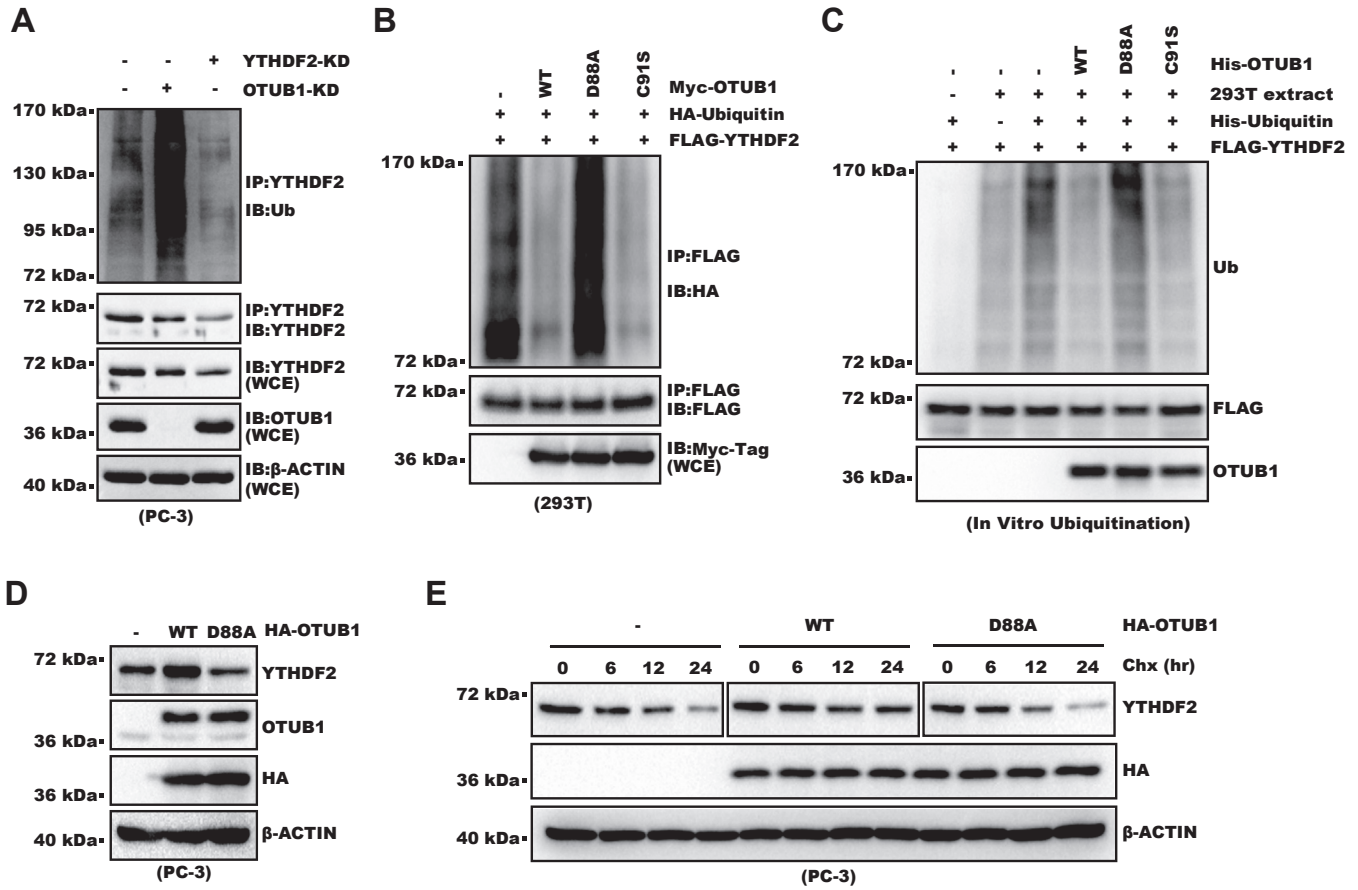

Figure 2. OTUB1 decreases YTHDF2 ubiquitination independent of the DUB activity. *A*, Ctrl, OTUB1-KD, or YTHDF2-KD PC-3 cells were analyzed with IP-WB as indicated. "Ub" denotes ubiquitin. *B*, 2 μg FLAG-YTHDF2, HA-ubiquitin, and Myc-OTUB1 plasmids were cotransfected into HEK-293T cells. Cells were analyzed with IP-WB as indicated. *C*, the result of the *in vitro* ubiquitination reaction as analyzed with WB. FLAG-YTHDF2 immunopurified from transfected HEK-293T cells was used as the substrate. It was incubated *in vitro* with recombinant His-ubiquitin and His-OTUB1. Then HEK-293T cell extract was added as a source of E2 and E3. "Ub" denotes ubiquitin. *D*, HA-OTUB1 WT or D88A mutant was expressed in PC-3 cells. WCE were analyzed with WB. *E*, HA-OTUB1 WT or D88A mutant was expressed in PC-3 cells. Cells were treated with 25 μg/ml Chx for different time. WCE were analyzed with WB. For YTHDF2, separate exposures for control and HA-OTUB1 cells were presented to make the signals of "Chx 0 h" comparable and facilitate the comparison of protein stability. Chx, cycloheximide; HA, hemagglutinin; IP, immunoprecipitation; KD, knock down; OTUB1, OUT domain–containing ubiquitin aldehyde-binding protein 1; PRSS8, protease serine S1 family member 8; WB, Western blot; WCE, whole-cell extract; YTHDF2, YTH domain–containing family protein 2.

study with cell counting, CCK-8, and colony-formation assay in three different cell lines (Figs. 3, *A–C* and S3, *A* and B). We next investigated whether the regulation of YTHDF2 mediated this effect of OTUB1. First, we examined the effect of YTHDF2 on cell proliferation. Cell counting, CCK-8, and colony-formation assay all showed YTHDF2 was required for cell proliferation in all three cell lines tested, which was consistent with previous reports in prostate cancer cells (19, 20) (Figs. 3, *D–F* and S3, *C* and D). Importantly, introducing exogenous YTHDF2 recovered proliferation of OTUB1-KD cells (Figs. 3, *G* and *H* and S3*E*), supporting YTHDF2 as an important mediator of the proliferation-promoting function of OTUB1.

OTUB1-YTHDF2 decreases PRSS8 mRNA level

Next, we went on to explore the potential effector downstream of the OTUB1–YTHDF2 axis. As changing mRNA stability was recognized as the main effect of YTHDF2, we analyzed published transcriptome change in YTHDF2-KD cells and m6A RNA immunoprecipitation (RIP)-sequencing data in PC-3 cells (19) to identify m6A-modified genes that are upregulated by YTHDF2-KD. Twenty nine genes were filtered out based on these criteria (Table S1). We then examined with real-time RT-PCR whether the mRNA levels of several candidate genes were also upregulated by OTUB1-KD (Fig. S4, *A–F*). These genes were chosen due to their reported connection to cancer (46–49). This analysis pipeline identified PRSS8 as a candidate, the mRNA level of which increased upon YTHDF2-KD or OTUB1-KD (Figs. 4, *A* and *B* and S4, *A–D*). PRSS8 encodes a serine protease and its protein level in the prostate was shown to be dozens of folds higher than in other tissues (40). We found that the PRSS8 protein level was also increased by YTHDF2-KD or OTUB1-KD (Figs. 4, *C* and *D* and S4, *G* and *H*). Importantly, introducing YTHDF2 into OTUB1-KD cells counteracted the upregulation of PRSS8 mRNA and protein, indicating that YTHDF2 mediated the effect of OTUB1 on PRSS8 (Figs. 4, *E* and *F* and S4*I*). These data identified that PRSS8 expression was repressed by the OTUB1–YTHDF2 axis.

YTHDF2 promotes PRSS8 mRNA degradation in an m6A-dependent manner

We found that YTHDF2 decreased PRSS8 mRNA level (Fig. 4). We next investigated the underlying mechanism.

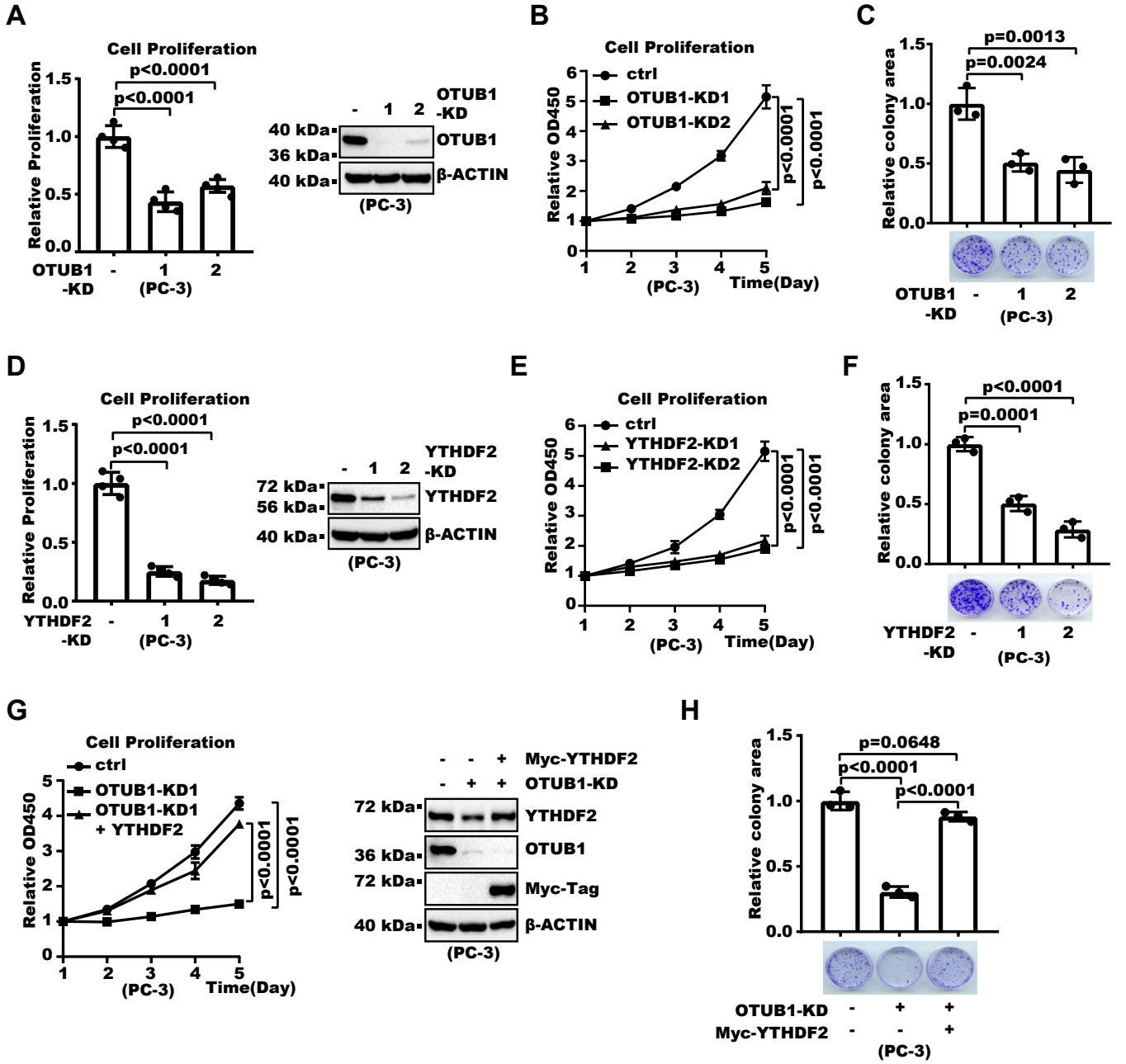

Figure 3. OTUB1 promotes prostate cancer cell proliferation through YTHDF2. *A*, *left*: relative proliferation during 3 days. The proliferation of control or OTUB1-KD PC-3 cells was analyzed with cell counting. Error bars denote the SD of four biological replicates. *p* values were from one-way ANOVA. The *right* shows WB results for WCE. *B*, proliferation of control or OTUB1-KD cells was analyzed with CCK-8. Shown are cell growth curves during 4 days. Error bars denote the SD of six biological replicates. *p* values were from two-way ANOVA. *C*, 1000 control or OTUB1-KD cells were seeded into 3.5 cm dishes. Fourteen days later, cells were fixed and stained with crystal violet. In the *bar graph*, error bars denote the SD of three biological replicates, and all data was normalized to the first group. *p* values were from one-way ANOVA. Below the *bar graph* shows the result of a representative experiment. *D*, *left*: relative proliferation during 4 days. Proliferation of control or YTHDF2-KD cells was analyzed with cell counting. Error bars denote the SD of four biological replicates. *p* values were from one-way ANOVA. The *right* shows WB results for WCE. *E*, proliferation of Control or YTHDF2-KD cells was analyzed with CCK-8. Shown are cell growth curves during 4 days. Error bars denote the SD of six biological replicates. *p* values were from two-way ANOVA. *F*, 1000 control or YTHDF2-KD cells were seeded into 3.5 cm dishes. Eighteen days later, cells were fixed and stained with crystal violet. In the *bar graph*, error bars denote the SD of three biological replicates, and all data was normalized to the first group. *p* values were from one-way ANOVA. Below the *bar graph* shows the result of a representative experiment. *G*, YTHDF2 was overexpressed in OTUB1-KD cells. On the *left*, the proliferation of Control, OTUB1-KD and "OTUB1-KD + YTHDF2" cells was analyzed with CCK-8. Shown are proliferation curves during 4 days. Error bars denote the SD of six biological replicates. *p* values were from two-way ANOVA. On the right is the WB result for WCE. *H*, YTHDF2 was overexpressed in OTUB1-KD cells. Five hundred cells were seeded into 3.5 cm dishes. Twelve days later, cells were fixed and stained with crystal violet. In the *bar graph*, error bars denote the SD of three biological replicates, and all data was normalized to the first group. *p* values were from one-way ANOVA. Below the *bar graph* shows the result of a representative experiment. KD, knock down; OTUB1, OUT domain–containing ubiquitin aldehyde-binding protein 1; WB, Western blot; WCE, whole-cell extract; YTHDF2, YTH domain–containing family protein 2.

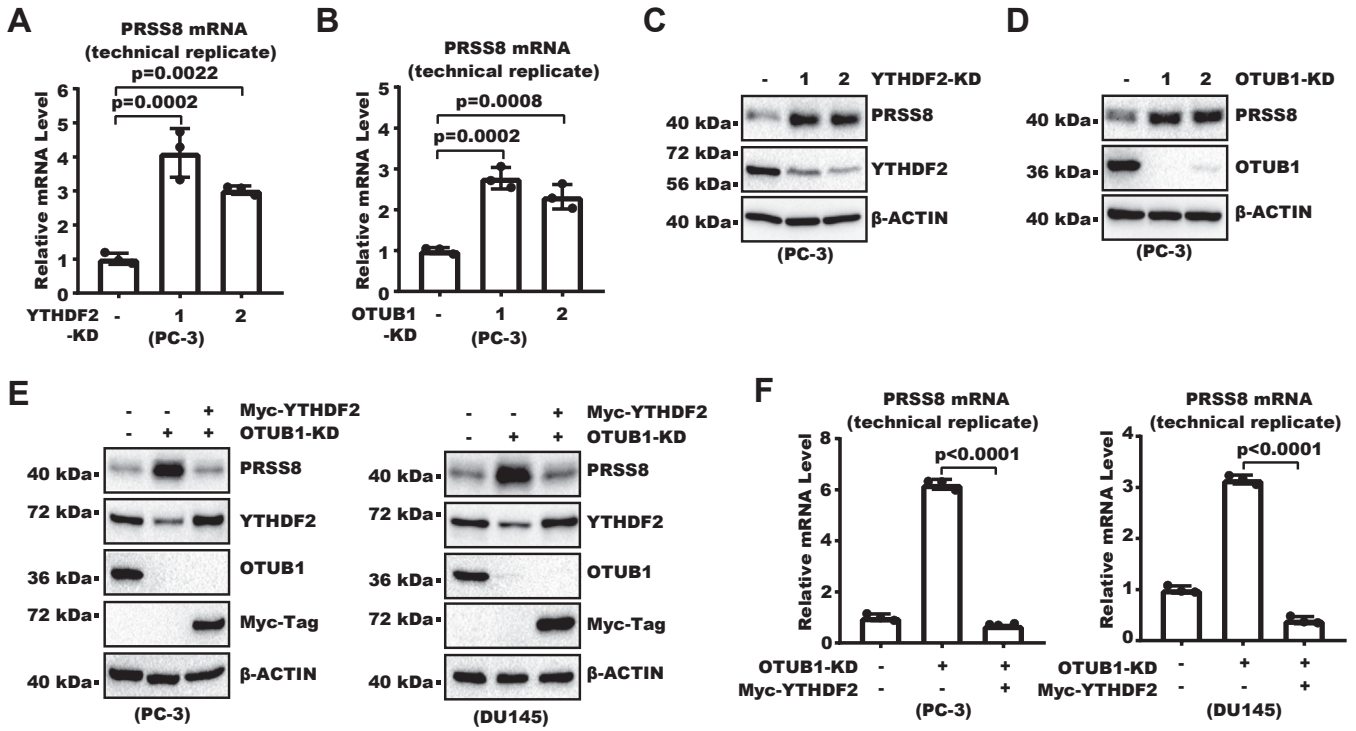

Figure 4. OTUB1-YTHDF2 regulates PRSS8 mRNA level. *A*, control or YTHDF2-KD cells were analyzed with real-time RT-PCR. Shown are relative PRSS8 mRNA levels normalized to β-actin. Error bars denote the SD of three technical replicates. *p* values were from one-way ANOVA. The result from a second independent experiment is shown in the Fig. S4*A*. *B*, control or OTUB1-KD cells were analyzed with real-time RT-PCR. Shown are relative PRSS8 mRNA levels normalized to β-actin. Error bars denote the SD of three technical replicates. *p* values were from one-way ANOVA. The result from a second independent experiment is shown in the Fig. S4*B*. *C*, WCE of Control or YTHDF2-KD PC-3 cells were analyzed with WB. *D*, WCE of control or OTUB1-KD PC-3 cells were analyzed with WB. *E*, Myc-YTHDF2 was expressed in OTUB1-KD cells. WCE of control, OTUB1-KD, and "OTUB1-KD + YTHDF2" cells were analyzed with WB. *F*, Myc-YTHDF2 was overexpressed in OTUB1-KD cells. Control, OTUB1-KD, and "OTUB1-KD + YTHDF2" cells were analyzed with real-time RT-PCR. Shown are relative PRSS8 mRNA levels normalized to β-ACTIN. Error bars denote the SD of three technical replicates. *p* values were from one-way ANOVA. The result from a second independent experiment is shown in the Fig. S4*I*. KD, knock down; OTUB1, OUT domain–containing ubiquitin aldehyde-binding protein 1; PRSS8, protease serine S1 family member 8; WB, Western blot; WCE, whole-cell extract; YTHDF2, YTH domain–containing family protein 2.

YTHDF2 was shown to bind mRNA and promote its degradation in an m6A-dependent manner (10). We performed RIP with YTHDF2 antibody to examine whether YTHDF2 bound to PRSS8 mRNA. The result showed PRSS8 mRNA was pulled down by YTHDF2 antibody in contrast to nonspecific IgG (Figs. 5*A* and S5, *A* and *B*), indicating YTHDF2 binds PRSS8 mRNA. Two experiments were performed to examine whether such binding is dependent on m6A modification. Firstly, RIP was performed with YTHDF2 antibody in METTL14-KD cells. The result showed that METTL14-KD decreased the binding between YTHDF2 and PRSS8 mRNA (Figs. 5*B* and S5, *C* and *D*). Secondly, RIP was performed for both YTHDF2 WT and W432A/W486A (W/A). As YTHDF2 recognized m6A through an aromatic cage comprising W432 and W486, W/A mutant was used to abolish YTHDF2 binding to m6A. The RIP result showed that the YTHDF2-W/A mutant had a diminished ability to bind PRSS8 mRNA (Figs. 5*C* and S5, *E* and *F*). These two RIP experiments together showed YTHDF2-bound PRSS8 mRNA in an m6A-dependent manner. We then treated cells with RNA synthesis inhibitor actinomycin for different time to examine whether YTHDF2 regulated PRSS8 mRNA stability. The result showed that YTHDF2-KD increased the stability of PRSS8 mRNA (Figs. 5*D* and S5, *G* and *H*). Importantly, the m6A level of PRSS8 mRNA was increased by knocking down OTUB1 or YTHDF2 (Figs. 5*E* and S5*I*). This indicated degradation of m6A-modified PRSS8 mRNA, compared to its nonmodified counterpart, was preferentially promoted by OTUB1 and YTHDF2. We reasoned if the effect of YTHDF2 on PRSS8 mRNA was through m6A recognition, it would be disrupted by W432A/W486A mutation. The result indeed showed W/A mutant failed to decrease the PRSS8 mRNA or protein level, in contrast to the YTHDF2 WT (Figs. 5*F* and S5, *J* and *K*). We further compared the effect of YTHDF2-WT on PRSS8 m6A level with that of W/A mutant. RIP with m6A antibody showed YTHDF2-WT preferentially promoted degradation of m6A-modified PRSS8 mRNA, while such effect was diminished for the YTHDF2-W/A mutant (Figs. 5*G* and S5, *L* and *M*). We further reasoned, that if m6A promoted PRSS8 mRNA degradation, PRSS8 expression should respond to change in m6A methyltransferase or demethylases. Indeed, PRSS8 expression was increased by knocking down METTL14, an indispensable component of the m6A methyltransferase complex (Figs 5*H* and S5*N*). Consistently, PRSS8 expression was decreased by knocking down m6A demethylase, FTO or ALKBH5 (Figs. 5, *I* and *J* and S5, *O* and *P*). Collectively, these data showed YTHDF2 bound to PRSS8 mRNA and promoted mRNA degradation in an m6A-dependent manner.

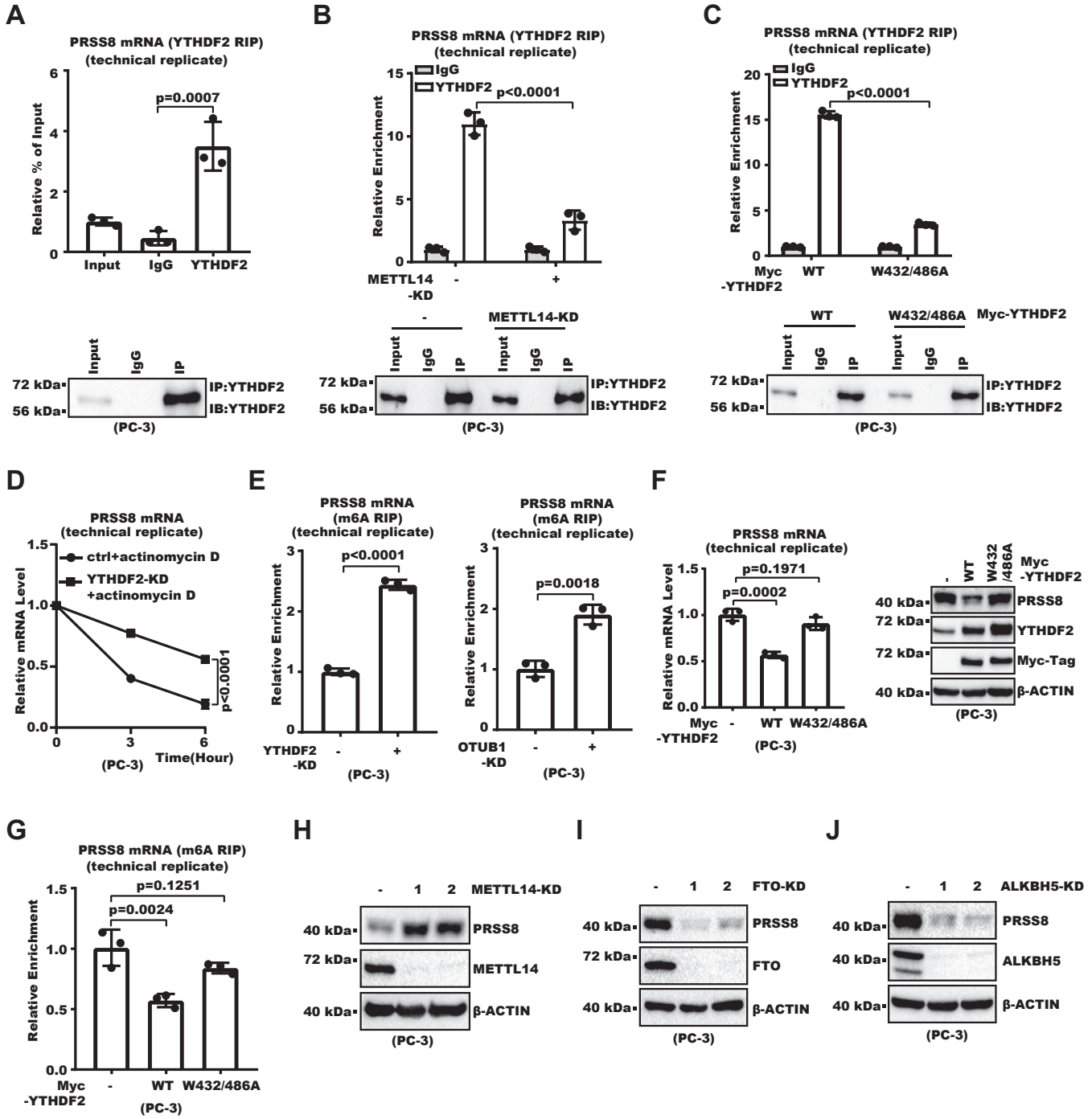

Figure 5. OTUB1-YTHDF2 regulates PRSS8 in an m6A-dependent manner. *A*, cell lysates were subject to RNA immunoprecipitation (RIP) with YTHDF2 antibody or nonspecific IgG. Immunoprecipitated RNA was then analyzed with real-time RT-PCR. Shown are levels of PRSS8 mRNA immunoprecipitated as normalized to 1% input. The companion WB results show the immunoprecipitation efficiency. Error bars denote the SD of three technical replicates. *p* values were from one-way ANOVA. "Input" denotes 1% input. The result from a second independent experiment is shown in the Fig. S5*A*. *B*, control or METTL14-KD cell lysates were subject to RNA immunoprecipitation (RIP) with YTHDF2 antibody or nonspecific IgG. Immunoprecipitated RNA was then analyzed with real-time RT-PCR. Shown are the relative PRSS8 mRNA levels as first normalized to 1% "input" in each group and then normalized to the IgG group. The companion WB results show the immunoprecipitation efficiency. Error bars denote the SD of three technical replicates. *p* values were from unpaired *t* test. "Input" denotes 1% input. The result from a second independent experiment is shown in the Fig. S5*C*. *C*, control, YTHDF2 WT, or W432A/W486A mutant cells were subject to RIP with YTHDF2 antibody or nonspecific IgG. Shown are relative PRSS8 mRNA levels as first normalized to 1% "input" in each group and then normalized to the IgG group. The companion WB results show the immunoprecipitation efficiency. Error bars denote the SD of three technical replicates. *p* values were from unpaired *t* test. "Input" denotes 1% input. The result from a second independent experiment is shown in the Fig. S5*E*. *D*, control or YTHDF2-KD cells were treated with 5 μg/ml actinomycin for different time. Cells were analyzed with real-time RT-PCR. Shown are the relative PRSS8 mRNA levels normalized to β-ACTIN. Error bars denote the SD of three technical replicates. *p* values were from two-way ANOVA. The result from a second independent experiment is shown in the Fig. S5*G*. *E*, control and YTHDF2-KD or OTUB1-KD cells were subject to RIP with m6A antibody. Immunoprecipitated RNA was analyzed with real-time RT-PCR. Shown are relative PRSS8 mRNA levels as first normalized to "input" in each group and then normalized to control cells. Error bars denote the SD of three technical replicates. *p* values were from unpaired *t* test. The result from a second independent experiment is shown in the Fig. S5*I*. *F*, YTHDF2 WT or W432A/W486A mutant was expressed in PC-3 cells. Cells were then analyzed with real-time RT-PCR

PRSS8 suppresses prostate cancer cell proliferation

PRSS8 was previously suggested to be a candidate tumor suppressor (50–57), but its role in prostate cancer remains unclarified. We compared the levels of PRSS8 in prostate cancer samples and paired normal samples with immunohistochemistry. The result showed that PRSS8 level was significantly lower in prostate cancer samples (Fig. 6*A*). We then examined whether PRSS8 regulated prostate cancer cell proliferation like OTUB1 and YTHDF2. Cell counting, CCK-8 assay, and colony-formation assay all showed that PRSS8 OE decreased prostate cancer cell proliferation (Figs. 6, *B–D* and S6, *A* and *B*). Consistently, PRSS8-KD increased prostate cancer cell proliferation (Figs. 6*E* and S6*C*). We further examined the effect in mouse models. First, we inoculated human PC3 cells into immuno-deficient mice. The result showed that PRSS8 OE significantly decreased tumor growth (Fig. 6, *F* and *G*). In addition, we inoculated mouse prostate cancer RM-1 cells to syngeneic C57BL/6 mice. The result again showed tumor growth was decreased by PRSS8 (Fig. 6, *H* and *I*). We went on to investigate how PRSS8 might regulate prostate cancer cell proliferation. We first examined whether the protease activity of PRSS8 was required by mutating the catalytic serine to alanine (58). The results from CCK-8 assay, cell counting, and colony-formation assay all showed this mutant inhibited cell proliferation to a similar extent with the wild-type (Figs. 6, *J* and *K* and S6, *D–F*). Collectively, these data indicate that PRSS8 inhibits prostate cancer cell proliferation in a protease activity-independent manner.

PRSS8 inhibits cell proliferation through the E-cadherin/β-catenin pathway

Intrigued by the potential mechanism of how PRSS8 repressed prostate cancer cell proliferation, we noticed PRSS8 OE changed the cell morphology from mesenchymal to epithelial-like with tighter cell–cell adhesion and less protrusion (Fig. S7*A*). Consistently, in both DU145 and PC-3 cells, WB detected a significant increase in E-cadherin protein level, a widely used marker for epithelial cells (Fig. S7*B*). In contrast, PRSS8-KD decreased the E-cadherin level (Fig. S7*C*). To mediate cell–cell adhesion, E-cadherin needs to localize to the plasma membrane. Indeed, immunofluorescence analysis detected significant increase in E-cadherin localization onto the plasma membrane in cells overexpressing PRSS8-WT or PRSS8-S238A (Fig 7*A*). Such an increase in E-cadherin was also confirmed in xenografts originating from PRSS8-overexpressing cells (Fig. 7*B*). Consistently, in TCGA prostate cancer cohort, PRSS8 positively correlated with E-cadherin protein level (Fig. 7*C*). Real-time RT-PCR indicated mRNA level of E-cadherin was not significantly changed by PRSS8 (Fig. S7*D*). Instead, the Chx treatment indicated that E-cadherin protein stability was increased by PRSS8 (Figs 7*D* and S7*E*). Of note, E-cadherin is not only an epithelial marker but also a potential tumor suppressor. E-cadherin sequesters β-catenin, a master oncogenic transcription coactivator, from entering the nucleus (59). Loss of E-cadherin expression is common in cancer (59, 60). Without E-cadherin, β-catenin localizes to the nucleus and initiates a protumor transcription program (61). So, we examined the β-catenin protein level in the cell nucleus after subcellular fractionation. The result showed that β-catenin localization to the nucleus was indeed decreased by PRSS8 (Fig. 7*E*). Immunofluorescence analysis on tumor sections from PRSS8-OE xenograft also detected decreased nuclear localization of β-catenin (Fig. 7*F*). We next examined whether the correlation between PRSS8 and β-catenin activity also existed in clinic samples. TCGA prostate cancer samples were divided into "PRSS8 high" and "PRSS8 low" groups and differential gene expression analysis was performed. Subsequent gene set enrichment analysis (GSEA) on the result showed the β-catenin pathway was downregulated in the "PRSS8 high" group (Fig. 7*G*). As another parametric measurement of β-catenin activity, the β-catenin activation score as defined previously was adopted (62). Analysis again showed PRSS8 negatively correlated with β-catenin activation score in TCGA prostate cancer samples (Fig. 7*H*). We then examined whether the effect of PRSS8 on β-catenin was indeed mediated by E-cadherin. We overexpressed PRSS8 in E-cadherin KD cells. The result showed that E-cadherin KD diminished the effect of PRSS8 on β-catenin (Figs 7*I* and S7*F*). Altogether these results show that the E-cadherin/β-catenin pathway is involved in the cell proliferation inhibition by PRSS8.

PRSS8 mediates the effect of OTUB1-YTHDF2 on prostate cancer cell proliferation

We further determined whether the decrease in PRSS8 mediated the effect of OTUB1 and YTHDF2 on prostate cancer cell proliferation. In YTHDF2-KD cells, suppressing PRSS8 partially restored cell proliferation as shown by CCK-8 assay and colony-formation assay (Figs. 8, *A* and *B* and S8, *A* and B). β-catenin nuclear localization was found to be decreased by PRSS8 (Fig. 7). Consistently, here in YTHDF2-KD cells, we found β-catenin localization to the nucleus was also decreased, which was largely restored upon PRSS8 KD (Fig. S8*C*). These results showed that PRSS8 was a key mediator of YTHDF2's effects on cell proliferation and β-catenin cytoplasm/nuclear distribution. As in YTHDF2-KD cells,

(*left*) or WB (*right*). Error bars denote the SD of three technical replicates. *p* values were from one-way ANOVA. The result from a second independent experiment is shown in the Fig. S5*J*. *G*, YTHDF2 WT or W432A/W486A mutant was expressed in PC-3 cells. Cells were subject to RIP with m6A antibody. Immunoprecipitated RNA was analyzed with real-time RT-PCR. Shown is relative PRSS8 mRNA as first normalized to "input" in each group and then normalized to the control group. Error bars denote the SD of three technical replicates. *p* values were from one-way ANOVA. The result from a second independent experiment is shown in the Fig. S5*L*. *H*, METTL14 was knocked down with shRNA. WCE were analyzed with WB. *I*, fat mass and obesity-associated protein was knocked down with shRNA. WCE were analyzed with WB. *J*, ALKBH5 was knocked down with shRNA. WCE were analyzed with WB. KD, knock down; m6A, methylation of adenine N6; OTUB1, OUT domain–containing ubiquitin aldehyde-binding protein 1; PRSS8, protease serine S1 family member 8; WB, Western blot; WCE, whole-cell extract; YTHDF2, YTH domain–containing family protein 2.

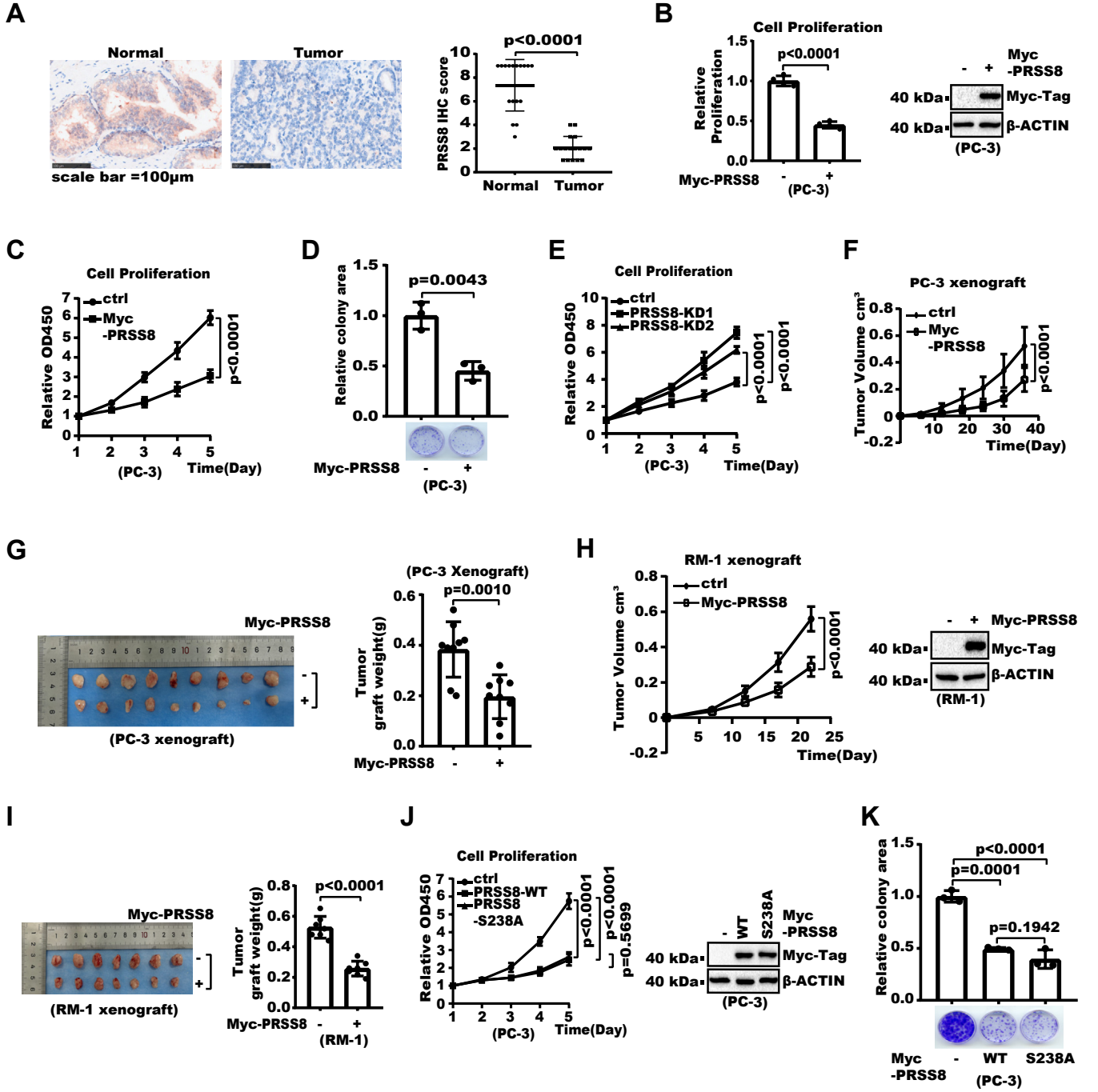

Figure 6. PRSS8 is a tumor suppressor gene in prostate cancer. *A*, 17 prostate sample slides containing both cancer tissue and adjacent normal tissue were analyzed with immunohistochemistry (IHC) with PRSS8 antibody. The *left* shows representative images from a representative slide. On the *right*, IHC results for normal tissues and cancer tissues were scored separately. The *p* value was from paired *t* test. *B*, PRSS8 was overexpressed in PC-3 cells. Shown on the *left* is the relative proliferation over 4 days as analyzed with cell counting. Error bars denote the SD of four biological replicates. *p* values were from unpaired *t* test. Shown on the *right* are WB results. *C*, PRSS8 was overexpressed in PC-3 cells. Cell proliferation during 4 days was analyzed with CCK-8. *D*, 500 control or PRSS8-overexpressing PC-3 cells were seeded into 3.5 cm dishes. Fourteen days later, cells were fixed and stained with crystal violet. In the *bar graph*, error bars denote the SD of three biological replicates, and all data was normalized to the control group. *p* values were from unpaired *t* test. Below the *bar graph* shows the result of a representative experiment. *E*, PRSS8 was knocked down in PC-3 cells. Cell proliferation was analyzed with CCK-8 over 4 days. Error bars denote the SD of six biological replicates. *p* values were from two-way ANOVA. *F*, 4×10^6 control or PRSS8-overexpressing PC-3 cells were inoculated to immuno-deficient mice. Shown are the tumor growth curves. Error bars denote the SD of nine mice. *p* values were from two-way ANOVA. *G*, PC-3 xenograft tumors from mice as in (*F*) were collected at the endpoint, photographed (*left*) and weighed (*right*). The *p* value was from unpaired *t* test. *H*, 5×10^5 control or PRSS8-overexpressing RM-1 cells were inoculated to syngeneic C57BL/6 mice. Shown on the *left* are the tumor growth curves. Error bars denote the SD of seven mice. *p* values were from two-way ANOVA. Shown on the *right* are WB results. *I*, RM-1 xenograft tumors from mice as in (*H*) were collected at the endpoint, photographed (*left*) and weighed (*right*). The *p* value was from unpaired *t* test. *J*, PRSS8 WT or S238A mutant was expressed in PC-3 cells. Shown on the *left* are cell growth curves during 4 days. Cell proliferation was analyzed with CCK-8. Error bars denote the SD of six biological replicates. *p* values were from two-way ANOVA. Shown on the *right* are WB results. *K*, PRSS8 WT or S238A mutant was expressed in PC-3 cells. One thousand control or PRSS8-overexpressing cells were seeded into 3.5 cm dishes. Twenty two days later, cells were fixed and stained with crystal violet. In the *bar graph*, error bars denote the SD of three biological replicates, and all data was normalized to the first group. *p* values were from one-way ANOVA. Below the *bar graph* shows the result of a representative experiment. PRSS8, protease serine S1 family member 8; WB, Western blot.

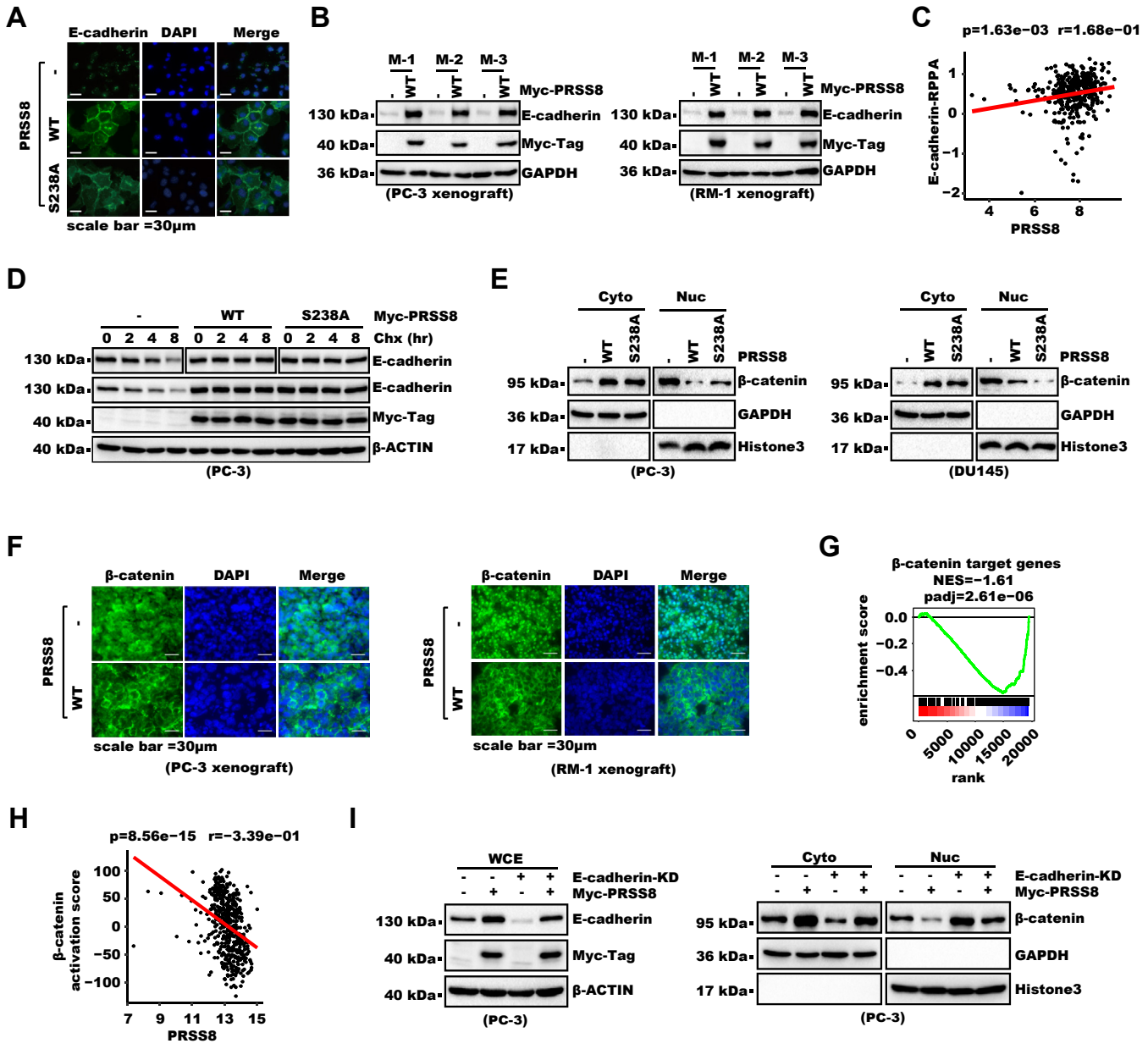

Figure 7. PRSS8 inhibits cell proliferation through the E-cadherin/β-catenin pathway. *A*, PRSS8 WT or S238A mutant was expressed in DU145 cells. Cells were analyzed with immunofluorescence with E-cadherin antibody, while nuclei were counterstained with DAPI. *B*, WCE were generated from Xenograft tumors from mice as in (Fig. 6, *G* and *I*). Shown are WB results. *C*, linear regression analysis for the correlation between PRSS8 and E-cadherin protein levels in patient samples from the TCGA prostate cancer cohort. The "r" denotes the Pearson correlation coefficient. *D*, PRSS8 WT or S238A mutant was expressed in PC-3 cells. Cells were treated with 25 μg/ml Chx at different time. WCE were analyzed with WB. The E-cadherin blot at the *top* was from the same blot as the one *below* but the presented images were from different exposure time to make the signals of "Chx 0 h" comparable. *E*, PRSS8 WT or S238A mutant was overexpressed in PC-3 or DU145 cells. Cells were fractionated into cytosolic and nuclear fractions. Fractions were then analyzed with WB as shown with GAPDH and histone H3 as cytosolic and nuclear markers respectively. "Cyto" denotes the cytoplasmic fraction and "Nuc" denotes the nuclear fraction. *F*, tumor sections from PRSS8-overexpressing xenograft as in (Fig. 6, *G* and *I*) were analyzed with immunofluorescence. Tissues were stained for β-catenin (*green*) while nuclei were counterstained with DAPI (*blue*). Shown are representative images. *G*, TCGA prostate cancer samples were divided into PRSS8 "high" and "low" groups. Then differential gene expression analysis was performed to sort the genes based on the fold of change. GSEA analysis for the enrichment of β-catenin target genes was then performed. *H*, linear regression analysis for the correlation between PRSS8 level and β-catenin activation score in patient samples from the TCGA prostate cancer cohort. The "r" denotes Pearson correlation coefficient. *I*, PRSS8 was overexpressed in control or E-cadherin-KD PC-3 cells. On the *left* are WB results for WCE to validate gene expression or knockdown. On the *right*, cells were fractionated into cytosolic and nuclear fractions followed by WB as shown. GAPDH and histone H3 were used as cytosolic and nuclear markers respectively. Chx, cycloheximide; DAPI, 4′,6-diamidino-2-phenylindole; GSEA, gene set enrichment analysis; PRSS8, protease serine S1 family member 8; TCGA, The Cancer Genome Atlas; WB, Western blot; WCE, whole-cell extract.

similar effect of PRSS8-KD on cell proliferation was also detected in OTUB1-KD cells as evidenced by cell counting, CCK-8 and colony-formation assay (Figs. 8, *C–E* and S8, *D* and *E*). These results collectively supported that PRSS8 is a key effector of OTUB1-YTHDF2.

Discussion

OTUB1 antagonizes YTHDF2 ubiquitination

As a critical mediator of m6A function, YTHDF2 is necessary for normal development, while dysregulation of YTHDF2

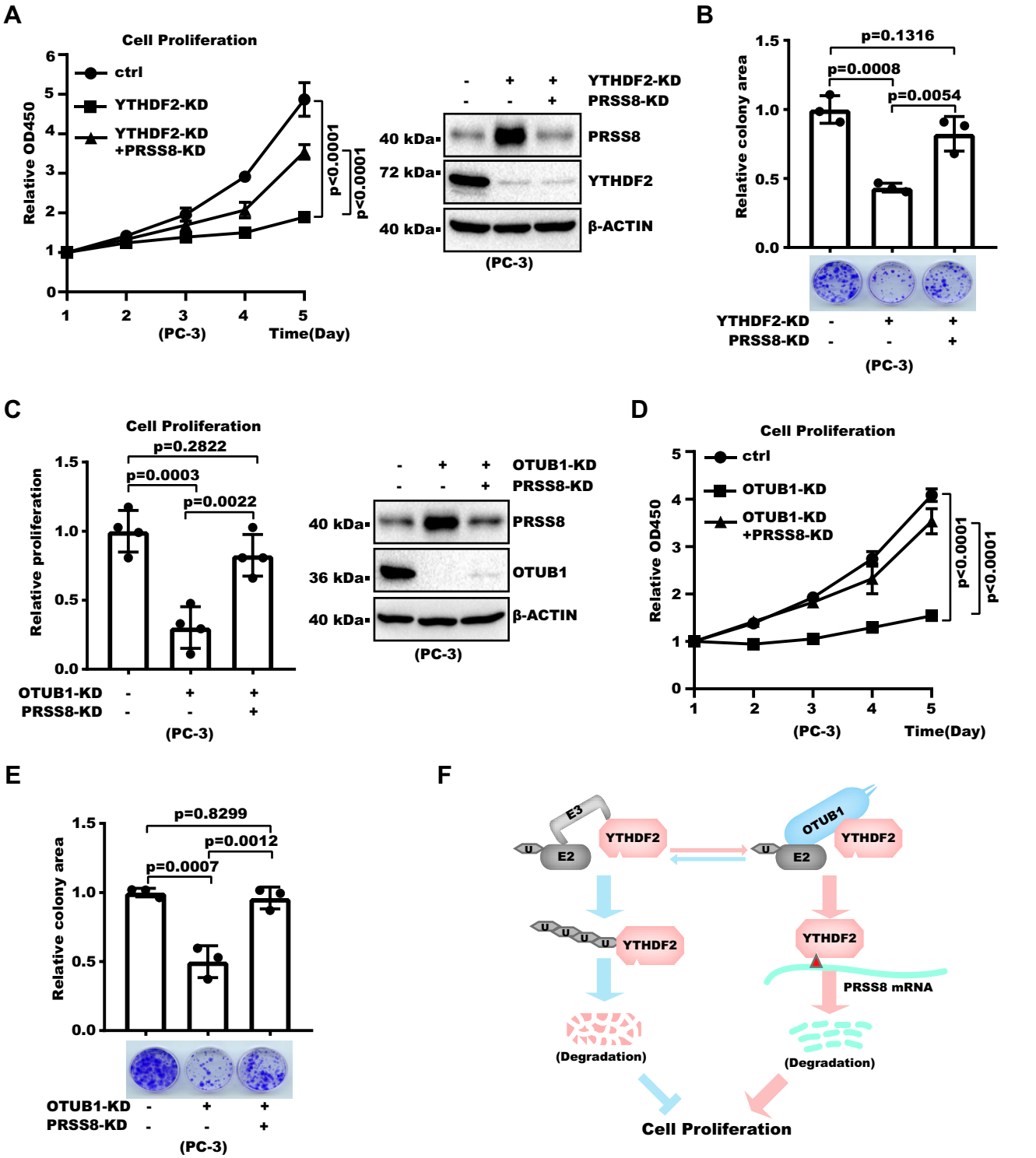

Figure 8. YTHDF2 and OTUB1 promote prostate cancer cell proliferation through PRSS8. *A*, PRSS8 was knocked down in control or YTHDF2-KD PC-3 cells. Shown on the *left* are proliferation curves during 4 days as determined with CCK-8. Error bars denote the SD of six biological replicates. *p* values were from two-way ANOVA. Shown on the *right* are WB results to validate gene expression and/or knockdown. *B*, PRSS8 was knocked down in control or YTHDF2-KD PC-3 cells. One thousand cells were seeded into 3.5 cm dishes. Fourteen days later, cells were fixed and stained with crystal violet. In the *bar graph*, error bars denote the SD of three biological replicates and all data was normalized to the first group. *p* values were from one-way ANOVA. Below the *bar graph* shows the result of a representative experiment. *C*, PRSS8 was knocked down in OTUB1-KD PC-3 cells. Shown on the *left* is relative cell proliferation during 4 days as analyzed with cell counting. Error bars denote the SD of four biological replicates. *p* values were from one-way ANOVA. Shown on the *right* are WB results for WCE to validate gene expression and/or knockdown. *D*, PRSS8 was knocked down in control or OTUB1-KD PC-3 cells. Shown on the *left* are proliferation curves during 4 days. Cell proliferation was analyzed with CCK-8. *E*, PRSS8 was knocked down in OTUB1-KD PC-3 cells. One thousand cells were seeded into 3.5 cm dishes. Twenty days later, cells were fixed and stained with crystal violet. In the *bar graph*, error bars denote the SD of three biological replicates and all data was normalized to the first group. *p* values were from one-way ANOVA. Below the *bar graph* shows the result of a representative experiment. *F*, working model of this study, where U denotes ubiquitin and ▲denotes m6A. OTUB1 inhibits YTHDF2 ubiquitination independent of its

contributes to multiple diseases including cancer (63). Regulation of the YTHDF2 protein level has proven critical for its biological function. Loss of a single allele of YTHDF2 in mice causes developmental defects and is partially lethal in inbred mice (17). On the other hand, OE of YTHDF2 plays a key role in various cancer types. Accordingly, recent studies have highlighted the mechanisms regulating the YTHDF2 protein level. YTHDF2 expression is subject to regulation at transcriptional, posttranscriptional, and posttranslational levels (20, 22, 23, 64–69). At the posttranslational level, phosphorylation, O-GlcNAcylation, and ubiquitination can regulate YTHDF2 protein stability (22, 23, 67, 68). Ubiquitination is generally considered dynamic and reversible. SKP2 and FBW7 can promote the ubiquitination of YTHDF2 as E3 ligases (22, 23). However, it remains elusive whether any deubiquitinase regulates YTHDF2. In this study, we uncover that OTUB1 is a key guardian for YTHDF2 protein stability. We demonstrate that OTUB1 represses YTHDF2 ubiquitination through a noncanonical mechanism, which is inhibiting ubiquitin transfer to YTHDF2. Several other proteins are regulated by OTUB1 through this mechanism (31). Interestingly, all of them were identified to interact with OTUB1, which might imply a mechanism for fine-tuning the specificity of OTUB1's noncanonical activity (31). Yet it remains unproven whether interaction with OTUB1 is indeed necessary for inhibition of ubiquitination. Such uncertainty could be resolved in the future by OTUB1 mutants that have specifically lost interaction with substrates. Importantly, as OTUB1 is overexpressed in multiple cancer types (36, 70), our study sheds mechanistic insight into the OE of YTHDF2 in cancer (Fig. 8*F*).

PRSS8 is a critical mediator of YTHDF2 function in prostate cancer

Cancer consists of a broad spectrum of highly diverse and heterogeneous diseases. Different cancer types may have different etiology and drivers. Consistently, different effectors of YTHDF2 have been identified in various cancer types. In this study, we identify PRSS8 as a key effector of YTHDF2 in prostate cancer cells. The significance of PRSS8 was previously shown in epithelial sodium channel activation and epidermis development (41, 42). Loss of Prss8 in mice leads to lethality within 60 h after birth due to dehydration and dysfunctional skin (41), which was suggested to be independent of its protease activity (71–73). Besides, a potential role of PRSS8 in cancer was implicated by its loss of expression in several cancer types (50–57). Loss of PRSS8 expression was partially attributed to DNA hypermethylation in bladder cancer, esophageal cancer, and breast cancer (50, 74, 75). A decrease in PRSS8 was observed in metastatic and castration-resistant prostate cancer as well (76, 77). However, the mechanism is not known. In this study, we find that PRSS8 expression is suppressed by the OTUB1–YTHDF2 axis. We show that YTHDF2 binds PRSS8 mRNA and promotes its degradation in an m6A-dependent manner. We further show a decrease in PRSS8 underlies the proproliferation by OTUB1-YTHDF2. This work not only uncovers a mechanism for decreased PRSS8 expression in prostate cancer but also highlights PRSS8 as a key mediator of OTUB1-YTHDF2 function in prostate cancer (Fig. 8*F*).

PRSS8 suppresses prostate cancer cell proliferation

Although loss of PRSS8 expression was reported in prostate cancer (76, 77), it remains unclear how PRSS8 affects prostate cancer cell biology. In this study, we first validate with paired normal and prostate cancer samples that PRSS8 expression is decreased in prostate cancer. We further show that PRSS8 inhibits prostate cancer cell proliferation with both cell culture and xenograft models. Mechanistically, we find PRSS8 promotes the epithelial morphology of prostate cancer cells, increases E-cadherin on the plasma membrane and decreases β-catenin in the cell nucleus. These findings corroborate that PRSS8 has a tumor-suppressive role in prostate cancer and implicate E-cadherin/β-catenin in the function of PRSS8. β-catenin functions both as a cell adherent junction protein and a coactivator for TCF-family transcription factors (78). As a coactivator, β-catenin promotes transcription of a protumor gene network. Aberrant activation of β-catenin contributes to the development and progression of various cancer types (79). Genomic mutation can contribute to β-catenin dysregulation in cancer. β-catenin is targeted by the anaphase promoting complex (APC) complex for proteasomal degradation, while mutations of APC or β-catenin disabling this mechanism are seen in many cancer types, including colorectal cancer and hepatocellular carcinoma (79). In addition, β-catenin is activated by other oncogenic signals. In prostate cancer, mutation of APC or β-catenin is not common. However, β-catenin clearly plays a role in prostate cancer development and progression. Knocking out APC or exon 3 of β-catenin leads to β-catenin activation and consequently prostate epithelial hyperplasia or prostate cancer (80). When combined with loss of phosphatase and tensin homolog, these mice develop invasive prostate cancer (81). Besides cell proliferation, β-catenin also promotes prostate cancer metastasis and resistance to castration, which is the major cause of prostate cancer-associated death (1, 82, 83). Accordingly, β-catenin is a promising target for cancer therapy. Nevertheless, β-catenin itself can be challenging to target (84). Alternatively, targeting pathways that lead to β-catenin activation may achieve similar effects. In this study, we find the OTUB1–YTHDF2–PRSS8 axis can promote the activation of β-catenin through repressing E-cadherin. This study provides insight into the mechanism of β-catenin activation in prostate cancer as well as β-catenin targeting drug discovery (81).

Experimental procedures

Cell culture

Androgen receptor-negative prostate cancer cell lines PC-3 (#CL-0185), DU145 (#CL-0075), and androgen-independent

DUB activity, which protects YTHDF2 from degradation. YTHDF2 in turn can bind PRSS8 mRNA and promotes its degradation, which increases cell proliferation. m6A, methylation of adenine N6; OTUB1, OUT domain–containing ubiquitin aldehyde-binding protein 1; PRSS8, protease serine S1 family member 8; WB, Western blot; KD, knock down; WCE, whole-cell extract; YTHDF2, YTH domain–containing family protein 2.

prostate cancer cell 22RV1 (#CL-0004) were purchased from Procell Life Science & Technology Co, Ltd and authenticated with short tandem repeat. HEK-293T cell was from Dr Shuguo Sun's Lab. The culture medium for PC-3 cell was Ham's F-12K (Procell Life Science & Technology Co, Ltd #PM150910) supplemented with 10% fetal bovine serum (PAN Biotech #ST30-3302). The culture medium for DU145 cell was minimum essential medium (Procell Life Science & Technology Co, Ltd #PM150410) supplemented with 10% fetal bovine serum. The culture medium for 22RV1 cell was RPMI-1640 (Procell Life Science & Technology Co, Ltd #PM150110) supplemented with 10% fetal bovine serum. The culture medium for HEK-293T cell was Dulbecco's modified Eagle's medium (Gibco #12800082) supplemented with 10% fetal bovine serum. Cells were cultured in a 37 °C incubator in 5% CO_2.

Western Blot

WB was performed as we described before (85, 86). Briefly, all protein samples were prepared in 1x loading buffer (62.5 mM Tris-Cl PH6.8, 2% SDS, 10% glycerol, 5% β-mercaptoethanol, 0.002% bromophenol blue) and then separated with SDS-PAGE. Afterward, the protein was blotted to a polyvinylidene fluoride membrane (Millipore #IPVH00010). polyvinylidene fluoride membranes were then incubated with primary antibodies and horseradish peroxidase (HRP)-conjugated secondary antibodies. Primary antibodies used are as follows: OTUB1 (Cell Signaling Technology #3783), YTHDF2 (Cell Signaling Technology #80014 for Figs. 1*C* and S1*A*, Proteintech #24744-1-AP for all the others), PRSS8 (Abcam #185236), GAPDH (Abclonal #AC033), β-actin (Abclonal #AC026), E-cadherin (BD Transduction Laboratories#610182), β-catenin (Cell Signaling Technology #9562), histone H3 (Abcam #ab1791), ubiquitin (Santa Cruz #sc-8017), YTHDF1 (Cell Signaling Technology #86463), YTHDF3 (Santa Cruz #sc-377119), METTL14 (Cell Signaling Technology #51104), ALKBH5 (Abcam #195377), FTO (Cell Signaling Technology #31687), hemagglutinin (HA)-tag (Cell Signaling Technology # 3724), FLAG-tag (Sigma #A8592), Myc-Tag (Santa Cruz #sc-40 for Figs. 1*H*, 2*B*, and S5*E*, Proteintech #16286-1-AP for all others). Secondary antibodies used include HRP-conjugated goat anti-rabbit IgG (H + L) (Jackson ImmunoResearch #111-035-144), HRP-conjugated goat anti-mouse IgG (H + L) (Jackson ImmunoResearch #115-035-062), HRP-conjugated monoclonal mouse anti-Rabbit IgG (light chain–specific) (Jackson ImmunoResearch #211-032-171), and HRP-conjugated goat anti-mouse IgG (light chain–specific) (Jackson ImmunoResearch #115-035-174).

Coimmunoprecipitation

Coimmunoprecipitation was performed as we previously reported (85, 86). Briefly, adherent cells were washed with cold PBS twice and then lysed in IPE150 buffer (20 mM Hepes pH 7.5, 150 mM NaCl, 0.5% NP40, 10% Glycerol). The cell lysate was cleared by centrifugation. The supernatant was then incubated with primary antibodies at 4 °C with rotation. Afterward, the antibody–antigen complex was captured with protein A/G-conjugated agarose beads (TransGen Biotech #DP501-01). Antibodies used for IP are YTHDF2 (Proteintech #24744-1-AP), OTUB1 (Cell Signaling Technology #3783) and Myc-Tag (Santa Cruz #sc-40). For FLAG-tag, anti-FLAG antibody-conjugated agarose beads (Sigma #A2220) were used for IP. Afterward, beads were washed three times with IPE150 buffer and protein was dissolved into 1x loading buffer for WB analysis.

Reverse transcription

Briefly, total RNA was extracted with TRIzol (Invitrogen #15596026) as the manufacturer recommended. Briefly, after medium removal, cells were lyzed in TRIzol. Then, 200 μl of chloroform per 1 ml of TRIzol was added to lysate and mixed thoroughly. After incubation at RT for 15 min, the mixture was centrifuged at 12,000 rpm for 15 min at 4 °C. Then supernatant was taken and mixed with equal volume of isopropanol to precipitate RNA. The mixture was then incubated for 10 min at RT followed by centrifugation at 12,000 rpm for 10 min at 4 °C. The supernatant was removed and the RNA pellet was washed twice with ice-cold 75% ethanol. RNA was then dried at RT and dissolved in nuclease-free water. The concentration and purity of RNA were measured with a NanoDrop One microvolume spectrometer (Thermo Fisher Scientific #701-058112). *A*260/*A*280 is typically within the range of 1.9 to 2.1 and *A* 260/230 is typically larger than 2.0. Approximately, 25 μg total RNA per million cells could be extracted from PC-3, 22RV1, and DU145 cells. One microgram RNA was then treated with DNase I (Thermo Fisher Scientific #EN0521) at 37 °C for 30 min to remove DNA contamination according to the manufacturer's instructions. Reverse transcription was typically performed right away with random primers and the ReverTra Ace quantitative real-time PCR RT-Kit (Toyobo #FSQ-101) as the manufacturer recommended. Briefly, decontaminated RNA was first mixed with 0.5 μg random primer, heated at 70 °C for 5 min, and then chilled on ice immediately. Next, 5x RT Buffer, RT Enzyme and nuclease-free water were added to the samples and mixed well. The RT reaction was carried out at 25 °C for 10 min, 37 °C for 15 min, and then terminated at 98 °C for 5 min. complementary DNA was stored at −20 °C.

Real-time PCR

Real-time PCR was performed with SYBR green real-time PCR Master Mix (Toyobo #QPK-201) on a CFX connect real-time PCR machine (Bio-Rad) as the manufacturer suggested. The amplification condition was as follows: initial denaturation at 95 °C for 3 min, followed by 40 cycles of 95 °C for 10 s, 55 °C for 30 s, and 72 °C for 15 s. PCR amplification efficiency was calculated by LinRegPCR (87). The sequences, expected product length, and amplification efficiency of PCR primers are all listed in Table S2.

KD and rescue expression

KD and rescue-expression were performed as we reported previously (85, 86). Briefly, KD was achieved with shRNA expressed by pLKO vector–based lentivirus transduction. Sense and antisense oligos were synthesized, annealed, and ligated to the pLKO vector linearized with EcoRI/AgeI. All other plasmids were made by ligating digested PCR products to vectors digested with compatible restriction enzymes. All PCR inserts were verified by Sanger sequencing. Used oligo sequences are listed in Table S2.

shRNA resistance was achieved by introducing synonymous mutation to the shRNA-targeting sequence. The sequences used are "acAacAaaCccAcaTatT" for OTUB1 and "TCctaTAGCgaAgaTgaCatCcaT" for YTHDF2 where capital letters denote synonymous mutation.

In vivo *ubiquitination assay*

For exogenous YTHDF2, 2.6 μg FLAG-YTHDF2 was cotransfected with 2.6 μg HA-ubiquitin and 2.6 μg Myc-OTUB1 into HEK-293T cells in a 6-cm dish. Two days later, cells were treated with 10 μM MG132 (MedChemExpress #HY-13259) for 4 h before collection into IPE150. The cell lysate was cleared by centrifugation and incubated with anti-FLAG antibody–conjugated agarose beads (Sigma #A2220) with rotation for 4 h at 4 °C. Beads were then washed with IPE1000 (20 mM Hepes pH 7.5, 1000 mM NaCl, 0.5% NP40, 10% glycerol) three times, 5 min each time. Afterward, immunoprecipitate was mixed with 1x loading buffer and analyzed with WB. For endogenous YTHDF2, the procedure was similar except the YTHDF2 antibody (Proteintech #24744-1-AP) and protein A/G–conjugated agarose beads (TransGen Biotech #DP501-01) were used for IP.

In vitro *ubiquitination assay*

Each 100 μl *in vitro* ubiquitination reaction contains 1x ubiquitination reaction buffer (25 mM Tris-Cl [pH 7.6], 2.5 mM MgCl2, 0.1 mM DTT), 4 mM ATP, 5 μg recombinant His-ubiquitin, 5 μg recombinant His-OTUB1, 70 μg HEK-293T cell lysate and immunopurified FLAG-YTHDF2. Components were prepared as follows. His-tagged OTUB1-WT, D88A, or C91S and His-ubiquitin were cloned into pET28A vector. The recombinant protein was expressed and purified from codon-plus *E. coli* strain (2nd Lab # EC1007S). HEK-293T cells were transfected with FLAG-YTHDF2 and collected into IPE150 2 days later. FLAG-YTHDF2 was immunopurified with anti-FLAG antibody–conjugated agarose beads (Sigma #A2220). Reactants were mixed and incubated at 37 °C for 2 h with rotation. Afterward, the reaction was terminated with 5x loading buffer and analyzed with WB.

In vitro *deubiquitination assay*

Each *in vitro* deubiquitination reaction contains 3 μg recombinant His-OTUB1 and immunopurified substrate (FLAG-YTHDF2 or Myc-PD-L1). The reaction was brought up to 40 μl with BC50 (20 mM Hepes pH 7.9, 50 mM NaCl, 10% glycerol). His-OTUB1 was purified from *E. coli* as described above. FLAG-YTHDF2 (or Myc-PD-L1) was cotransfected with HA-ubiquitin into HEK-293T cells. Cells were treated 2 days later with 10 μM MG132 for 4 h and then collected into IPE150 supplemented with 10 mM N-ethylmaleimide. The cell lysate was cleared by centrifugation. FLAG-YTHDF2 was immunoprecipitated with anti-FLAG antibody–conjugated agarose beads (Sigma #A2220). Myc-PD-L1 was immunoprecipitated with Myc-tag antibody (Santa Cruz #sc-40) and protein A/G–conjugated agarose beads (TransGen Biotech #DP501-01). Reactants were mixed well and incubated with rotation at 30 °C for 2 h. The reaction was terminated with 5x loading buffer and analyzed with WB.

YTHDF2 RIP

RIP was performed as previously reported with minor modifications (88). Briefly, 1×10^7 cells were washed with cold PBS twice and then lysed in 500 μl IPE150 supplemented with 200 U/ml RNase inhibitor (Promega #N2515). The cell lysate was cleared by centrifugation and the supernatant was incubated with 2 μg YTHDF2 antibody (Proteintech #24744-1-AP). Immunocomplex was captured with protein-A/G magnetic beads (MedChemExpress #HY-K0202). Beads were then washed with IPE150 supplemented with 100 U/ml RNase inhibitor (Promega #N2515) three times, 5 min each time. Then beads were aliquoted into two parts. One part was used for RNA extraction with TRIzol (Invitrogen #15596026) as the manufacturer suggested. Purified RNA was then subject to analysis with reverse transcription and real-time PCR. The other part of the immunoprecipitated material was then dissolved with 1x loading buffer for WB analysis.

m6A RIP

m6A RIP was performed as previously described with minor modifications (89). Total RNA of 2×10^7 cells was extracted with TRIzol (Invitrogen #15596026) as the manufacturer recommended. mRNA was then isolated from total RNA with PolyATtract mRNA isolation systems IV (Promega #Z5310) as the manufacturer suggested. Three micrograms mRNA was then incubated with premixed 5 μg m6A antibody (Cell Signaling Technology #56593) and 25 μl protein A/G–conjugated magnetic beads (MedChemExpress #HY-K0202) at 4 °C for 1 h with gentle rotation. Afterward, beads were washed with methylated RNA immunoprecipitation buffer (10 mM Tris pH 7.4, 150 mM NaCl, 0.1% NP-40, 100 U/ml RNase inhibition). TRIzol was then added to extract RNA. The purified RNA was then subject to analysis with reverse transcription and real-time PCR.

RNA stability assay

Cells were treated with 5 μg/ml actinomycin D (MedChemExpress #HY-17559) to block transcription for different time. Cells were directly lysed with TRIzol (Invitrogen #15596026) and total RNA was extracted as the manufacturer

recommended. RNA was then subject to reverse transcription and complementary DNA was analyzed with real-time PCR.

Subcellular fractionation

Subcellular fractionation was performed exactly as we described before (85, 86). Briefly, cells were first resuspended in hypotonic buffer (10 mM Hepes pH 7.9, 10 mM KCl, 0.5 mM DTT, 1.5 mM MgCl2). Afterward, NP40 was added to 0.2% final concentration and cells were vortexed vigorously to break the plasma membrane. Cells were then centrifuged with the pellet being nuclei and the supernatant being cytoplasm. Cytoplasmic and nuclear fractions were analyzed with WB.

Cell proliferation assay: CCK8 and cell counting

CCK8 assay was performed with a CCK-8 kit (MedChemExpress #HY-K0301) as the manufacturer recommended. Briefly, 1×10^3 cells were seeded into each well of a 96-well plate with 200 μl complete medium. Ten microliters CCK-8 was added to each well and incubated for 1 h. Optical absorbance at 450 nm was then measured with a Multiskan GO UV/Visible spectrophotometer (Thermo Fisher Scientific #51119300).

For cell counting, the same amount of cells were seeded into 3.5 cm dishes. Cells were counted 4 days later.

Clonogenesis

Cells were trypsinized and resuspended. A total of 1×10^3 cells were then seeded into each 3.5 cm dish. Cells were let grow for 2 weeks and the culture medium was refreshed every week. Afterward, cells were washed with PBS twice and fixed with methanol for 5 min. Then cells were stained with crystal violet (0.5% dissolved in methanol) for 10 min. Afterwards, the staining solution was discarded and cells were washed with distilled water five times. The dishes were let dry in the air and photos were later captured with a document scanner (Epson Perfection V550). Photos were then analyzed with the FIJI (https://imagej.net/software/fiji/) software package. First, images were turned into 8 bit. Then, the image color was inverted. Afterward, the background was subtracted with the rolling ball method. Then images were converted into binary files with the "dark background" option selected. Finally, the total area of colonies was measured with the "measure" tool. The same parameters were used across images.

Mouse xenograft

All animal studies were conducted at the animal facility of Huazhong University of Science and Technology and approved by the ethics committee of Tongji Medical College. A total of 4×10^6 control or PRSS8-overexpressing cells were resuspended in 1:1 mixture of PBS and matrigel (Corning #354248). Cells were then injected subcutaneously into the flanks of seven mice. For PC-3 cells, 6-week-old male BALB/c nude mice (Beijing Vital River Laboratory Animal Technology) were used. For RM-1 cells, 6-week-old male C57BL/6J mice (Beijing Vital River Laboratory Animal Technology) were used. All animals were housed at (21 ± 1 °C) with a 12 h light/12 h darkness cycle. All animals were acclimated to the new environment for at least 1 week. Food and water were available ad libitum. Tumor volume was estimated by the formula 0.5*L*W*W (L means long diameter, W means short diameter). Mice were euthanized before any estimated tumor volume reached 1000 mm^3. Tumors were then dissected and weighed.

Immunohistochemical staining

Leftover slides for 17 prostate cancer samples from pathology examination were provided by Peking University First Hospital. Each slide contains both cancer tissue and adjacent normal tissue. The use of patient samples was approved by the ethics committee of Peking University First Hospital with patients' consent and abided by the Declaration of Helsinki principles. Slides were analyzed with routine immunohistochemical staining. Briefly, slides were first dewaxed and rehydrated, and then treated with citrate buffer (Solarbio Life Science #C1032) for antigen retrieval. Slides were then blocked with 3% bovine serum albumin (Solarbio Life Science #A8020) for 30 min at 37 °C and then incubated with PRSS8 antibody (Abcam #227225). After washing, slides were incubated with HRP-conjugated secondary antibody (ZSGB-Bio #PV-9001). Slides were then incubated with DAB (ZSGB-Bio #ZLI-9017) to develop. Slides were transferred to PBS to stop developing before incubation with H&E Staining Solution (Beyotime Biotechnology #C0107). Slides were mounted into Neutral balsam (Solarbio Life Science #G8590). Images were taken with NanoZoomer S360 whole slide imaging scanner (Hamamatsu Photonics). Images were scored by an experienced pathologist. p values were calculated from paired two-tailed t test.

Immunofluorescence

Mouse tumor tissues embedded in OCT compound (Sakura Finetek Inc, #Sakura 4583) were cut into 8-μm frozen sections with LEICA CM1860 Cryostat Microtome. For immunofluorescence staining, frozen sections were fixed with 4% paraformaldehyde in PBS for 15 min at 4 °C. Frozen sections were then permeabilized with 0.5% Triton X-100. After washing with PBS, slides were blocked with 1% bovine serum albumin in 0.2% Tween-20 in PBS for 1 h at room temperature (RT). The sections were then incubated with β-catenin antibody (Abclonal #A19657) overnight at 4 °C. After washing three times with 0.2% Tween-20 in PBS, sections were incubated with Alexa Fluor 488–conjugated donkey anti-rabbit IgG secondary antibody (Jackson ImmunoResearch #711-545-152) at RT in dark for 1 h. Lastly, nuclei were counter-stained with 1.5 μM 4′,6-diamidino-2-phenylindole for 5 min. Sections were mounted onto glass slides in antifade fluorescence mounting medium (Abcam #AB104135).

Gene set enrichment analysis

GSEA analysis was performed as we previously described (90). RNA-Seq data for prostate cancer samples in The Cancer Genome Atlas (TCGA) program was downloaded from "https://gdc.cancer.gov/" in the form of STAR counts. Tumor

samples were divided into "high" and "low" groups based on the PRSS8 mRNA levels. Differential gene expression analysis comparing "high" *versus* "low" groups was then performed with the "DeSeq2" (https://bioconductor.org/packages/release/bioc/html/DESeq2.html) package in R (4.2.1). Protein coding genes were then ordered based on their fold of change. Then GSEA analysis for the preordered geneset was analyzed with the "fgsea" package with default parameters in R (4.2.1). GSEA plot was generated with the "ggsea" package in R (4.2.1).

Correlation analysis between PRSS8 and E-cadherin

TCGA RNA-Seq data was downloaded from "https://gdc.cancer.gov/" in the form of transcripts per million (TPM). Level-3 TCGA reverse phase protein array (RPPA) data was downloaded from the same source. TPM was log2-transformed with the formula $\log_2$ (TPM + 0.5). Afterward, Pearson correlation analysis was performed in R (4.2.1) for log2-transformed PRSS8 TPM and E-cadherin protein level from the RPPA data. All 351 prostate cancer samples with both TPM and RPPA data were included in the analysis.

Correlation analysis between PRSS8 and β-catenin activation score

The β-catenin activation score was calculated as reported previously (62). All β-catenin target genes assembled by Luke *et al* (62) were included to calculate the β-catenin activation score. Briefly, gene expression, as determined in the TCGA RNA-Seq dataset, were first normalized with "DESeq2" in R (4.2.1). All 497 prostate cancer samples with RNA-Seq data were included in the analysis. Then a β value was calculated for each gene in each sample. β value was calculated for each sample with the formula β = (expr-mean)/SD. Herein, "expr" denotes the expression of a specific gene in a specific sample, "mean" denotes the mean expression of this gene in all samples, and "SD" denotes the standard deviation of the expression level of this gene in all samples. Samples with β larger than 0.1 were given a score of 1 while those with β less than −0.1 were given a score of −1. Summarization of scores for all genes generates the β-catenin activation score for each sample. Afterward, Pearson correlation for PRSS8 mRNA level and β-catenin activation score was performed in R (4.2.1).

Statistical analysis

For CCK-8 assay, xenograft tumor growth curve and mRNA stability assay, p values were calculated from two-way ANOVA. p values for all other assays (cell proliferation, real-time PCR, tumor weight) were calculated by either t test or one-way ANOVA as specified in the Figure legends. For one-way ANOVA, Sidak statistical hypothesis testing was used to correct for multiple comparison as recommended by GraphPad Prism 8.0.2. (https://www.graphpad.com/) p values (or P-adjusted for multiple comparison) less than 0.05 were deemed significant. All error bars denote the SD with number of replicates specified in the Figure legends.

Data availability

Data underlying this article are available in the article and its online supplementary material.

Supporting information—This article contains supporting information.

Acknowledgments—We thank Dr Zhou J from the Department of Urology, Peking University First Hospital for providing prostate cancer sample slides.

Author contributions—X. Z., L. S., and T. S. conceptualization; X. Z., L. S., and T. S. methodology; X. Z., L. S., and T. S. formal analysis; X. Z., S. L., N. L., and Q. Z. investigation; X. Z., S. L., N. L., and Q. Z. validation; X. Z. visualization; L. S. and T. S. writing-original draft; X. Z., S. L., N. L., Q. Z., L. S., and T. S. writing-review and editing; L. S. and T. S. funding acquisition.

Funding and additional information—This work was supported by grants from the National Natural Science Foundation of China (32071296, 32371320, and 31871284 to L. S, 31971149 and 31800641 to T. S.) and Natural Science Foundation of Hubei Province of China (2022CFB251 to T. S).

Conflict of interest—The authors declare that they have no conflicts of interest with the contents of this article.

Abbreviations—The abbreviations used are: APC, anaphase promoting complex; Chx, cycloheximide; FTO, fat mass and obesity-associated protein; GSEA, gene set enrichment analysis; HA, hemagglutinin; HRP, horseradish peroxidase; IP, immunoprecipitation; KD, knockdown; m6A, methylation of adenine N6; OE, overexpression; OTUB1, OUT domain–containing ubiquitin aldehyde-binding protein 1; PRSS8, protease serine S1 family member 8; RIP, RNA immunoprecipitation; RPPA, reverse phase protein array; RT, room temperature; TCGA, The Cancer Genome Atlas; TPM, transcripts per million; YTHDF2, YTH domain–containing family protein 2; WB, Western blot.

References

1. Schmidt, K. T., Huitema, A. D. R., Chau, C. H., and Figg, W. D. (2021) Resistance to second-generation androgen receptor antagonists in prostate cancer. *Nat. Rev. Urol.* **18**, 209–226
2. Sung, H., Ferlay, J., Siegel, R. L., Laversanne, M., Soerjomataram, I., Jemal, A., *et al.* (2021) Global cancer Statistics 2020: GLOBOCAN Estimates of Incidence and mortality worldwide for 36 cancers in 185 Countries. *CA Cancer J. Clin.* **71**, 209–249
3. Ku, S. Y., Gleave, M. E., and Beltran, H. (2019) Towards precision oncology in advanced prostate cancer. *Nat. Rev. Urol.* **16**, 645–654
4. Huang, H., Weng, H., and Chen, J. (2020) m(6)A modification in coding and non-coding RNAs: roles and therapeutic Implications in cancer. *Cancer Cell* **37**, 270–288
5. Shi, H., Wei, J., and He, C. (2019) Where, when, and how: context-dependent functions of RNA methylation writers, readers, and erasers. *Mol. Cell* **74**, 640–650
6. Bokar, J. A., Shambaugh, M. E., Polayes, D., Matera, A. G., and Rottman, F. M. (1997) Purification and cDNA cloning of the AdoMet-binding subunit of the human mRNA (N6-adenosine)-methyltransferase. *RNA* **3**, 1233–1247
7. Wang, X., Feng, J., Xue, Y., Guan, Z., Zhang, D., Liu, Z., *et al.* (2016) Structural basis of N(6)-adenosine methylation by the METTL3-METTL14 complex. *Nature* **534**, 575–578

8. Garcias Morales, D., and Reyes, J. L. (2021) A birds'-eye view of the activity and specificity of the mRNA M(6) A methyltransferase complex. *Wiley Interdiscip. Rev. RNA* **12**, e1618
9. Dominissini, D., Moshitch-Moshkovitz, S., Schwartz, S., Salmon-Divon, M., Ungar, L., Osenberg, S., *et al.* (2012) Topology of the human and mouse m6A RNA methylomes revealed by m6A-seq. *Nature* **485**, 201–206
10. Wang, X., Lu, Z., Gomez, A., Hon, G. C., Yue, Y., Han, D., *et al.* (2014) N6-methyladenosine-dependent regulation of messenger RNA stability. *Nature* **505**, 117–120
11. Li, F., Zhao, D., Wu, J., and Shi, Y. (2014) Structure of the YTH domain of human YTHDF2 in complex with an m(6)A mononucleotide reveals an aromatic cage for m(6)A recognition. *Cell Res.* **24**, 1490–1492
12. Theler, D., Dominguez, C., Blatter, M., Boudet, J., and Allain, F. H. (2014) Solution structure of the YTH domain in complex with N6-methyladenosine RNA: a reader of methylated RNA. *Nucleic Acids Res.* **42**, 13911–13919
13. Xu, C., Wang, X., Liu, K., Roundtree, I. A., Tempel, W., Li, Y., *et al.* (2014) Structural basis for selective binding of m6A RNA by the YTHDC1 YTH domain. *Nat. Chem. Biol.* **10**, 927–929
14. Adams-Cioaba, M. A., and Min, J. (2009) Structure and function of histone methylation binding proteins. *Biochem. Cell Biol.* **87**, 93–105
15. Lasman, L., Krupalnik, V., Viukov, S., Mor, N., Aguilera-Castrejon, A., Schneir, D., *et al.* (2020) Context-dependent functional compensation between Ythdf m(6)A reader proteins. *Genes Dev.* **34**, 1373–1391
16. Dixit, D., Prager, B. C., Gimple, R. C., Poh, H. X., Wang, Y., Wu, Q., *et al.* (2021) The RNA m6A reader YTHDF2 Maintains Oncogene expression and is a targetable dependency in glioblastoma stem cells. *Cancer Discov.* **11**, 480–499
17. Li, M., Zhao, X., Wang, W., Shi, H., Pan, Q., Lu, Z., *et al.* (2018) Ythdf2-mediated m(6)A mRNA clearance modulates neural development in mice. *Genome Biol.* **19**, 69
18. Chen, X., Zhou, X., and Wang, X. (2022) m(6)A binding protein YTHDF2 in cancer. *Exp. Hematol. Oncol.* **11**, 21
19. Li, J., Xie, H., Ying, Y., Chen, H., Yan, H., He, L., *et al.* (2020) YTHDF2 mediates the mRNA degradation of the tumor suppressors to induce AKT phosphorylation in N6-methyladenosine-dependent way in prostate cancer. *Mol. Cancer* **19**, 152
20. Li, J., Meng, S., Xu, M., Wang, S., He, L., Xu, X., *et al.* (2018) Down-regulation of N(6)-methyladenosine binding YTHDF2 protein mediated by miR-493-3p suppresses prostate cancer by elevating N(6)-methyladenosine levels. *Oncotarget* **9**, 3752–3764
21. Varshavsky, A. (2012) The ubiquitin system, an immense realm. *Annu. Rev. Biochem.* **81**, 167–176
22. Xu, F., Li, J., Ni, M., Cheng, J., Zhao, H., Wang, S., *et al.* (2021) FBW7 suppresses ovarian cancer development by targeting the N(6)-methyladenosine binding protein YTHDF2. *Mol. Cancer* **20**, 45
23. Fei, Q., Zou, Z., Roundtree, I. A., Sun, H. L., and He, C. (2020) YTHDF2 promotes mitotic entry and is regulated by cell cycle mediators. *PLoS Biol.* **18**, e3000664
24. Reyes-Turcu, F. E., Ventii, K. H., and Wilkinson, K. D. (2009) Regulation and cellular roles of ubiquitin-specific deubiquitinating enzymes. *Annu. Rev. Biochem.* **78**, 363–397
25. Nijman, S. M., Luna-Vargas, M. P., Velds, A., Brummelkamp, T. R., Dirac, A. M., Sixma, T. K., *et al.* (2005) A genomic and functional inventory of deubiquitinating enzymes. *Cell* **123**, 773–786
26. Keusekotten, K., Elliott, P. R., Glockner, L., Fiil, B. K., Damgaard, R. B., Kulathu, Y., *et al.* (2013) OTULIN antagonizes LUBAC signaling by specifically hydrolyzing Met1-linked polyubiquitin. *Cell* **153**, 1312–1326
27. Edelmann, M. J., Iphofer, A., Akutsu, M., Altun, M., di Gleria, K., Kramer, H. B., *et al.* (2009) Structural basis and specificity of human otubain 1-mediated deubiquitination. *Biochem. J.* **418**, 379–390
28. Hu, M., Li, P., Li, M., Li, W., Yao, T., Wu, J. W., *et al.* (2002) Crystal structure of a UBP-family deubiquitinating enzyme in isolation and in complex with ubiquitin aldehyde. *Cell* **111**, 1041–1054
29. Komander, D., and Rape, M. (2012) The ubiquitin code. *Annu. Rev. Biochem.* **81**, 203–229
30. Nakada, S., Tai, I., Panier, S., Al-Hakim, A., Iemura, S., Juang, Y. C., *et al.* (2010) Non-canonical inhibition of DNA damage-dependent ubiquitination by OTUB1. *Nature* **466**, 941–946
31. Wu, M., Sun, L., and Song, T. (2024) OTUB1-mediated inhibition of ubiquitination: a growing list of effectors, multiplex mechanisms and versatile functions. *Front. Mol. Biosci.* **10**, 1261273
32. Zhao, L., Wang, X., Yu, Y., Deng, L., Chen, L., Peng, X., *et al.* (2018) OTUB1 protein suppresses mTOR complex 1 (mTORC1) activity by deubiquitinating the mTORC1 inhibitor DEPTOR. *J. Biol. Chem.* **293**, 4883–4892
33. Wu, Q., Huang, Y., Gu, L., Chang, Z., and Li, G. M. (2021) OTUB1 stabilizes mismatch repair protein MSH2 by blocking ubiquitination. *J. Biol. Chem.* **296**, 100466
34. Jahan, A. S., Biquand, E., Munoz-Moreno, R., Le Quang, A., Mok, C. K., Wong, H. H., *et al.* (2020) OTUB1 is a key regulator of RIG-I-dependent immune signaling and is targeted for proteasomal degradation by Influenza A NS1. *Cell Rep.* **30**, 1570–1584
35. Sun, X. X., Challagundla, K. B., and Dai, M. S. (2012) Positive regulation of p53 stability and activity by the deubiquitinating enzyme Otubain 1. *EMBO J.* **31**, 576–592
36. Liao, Y., Yang, M., Wang, K., Wang, Y., Zhong, B., and Jiang, N. (2022) Deubiquitinating enzyme OTUB1 in immunity and cancer: good player or bad actor? *Cancer Lett.* **526**, 248–258
37. Ruiz-Serrano, A., Monne Rodriguez, J. M., Gunter, J., Sherman, S. P. M., Jucht, A. E., Fluechter, P., *et al.* (2021) OTUB1 regulates lung development, adult lung tissue homeostasis, and respiratory control. *FASEB J.* **35**, e22039
38. Iglesias-Gato, D., Chuan, Y. C., Jiang, N., Svensson, C., Bao, J., Paul, I., *et al.* (2015) OTUB1 de-ubiquitinating enzyme promotes prostate cancer cell invasion in vitro and tumorigenesis in vivo. *Mol. Cancer* **14**, 8
39. Liao, Y., Wu, N., Wang, K., Wang, M., Wang, Y., Gao, J., *et al.* (2020) OTUB1 promotes progression and proliferation of prostate cancer via deubiquitinating and Stabling cyclin E1. *Front. Cell Dev. Biol.* **8**, 617758
40. Yu, J. X., Chao, L., and Chao, J. (1994) Prostasin is a novel human serine proteinase from seminal fluid. Purification, tissue distribution, and localization in prostate gland. *J. Biol. Chem.* **269**, 18843–18848
41. Leyvraz, C., Charles, R. P., Rubera, I., Guitard, M., Rotman, S., Breiden, B., *et al.* (2005) The epidermal barrier function is dependent on the serine protease CAP1/Prss8. *J. Cell Biol.* **170**, 487–496
42. Vallet, V., Chraibi, A., Gaeggeler, H. P., Horisberger, J. D., and Rossier, B. C. (1997) An epithelial serine protease activates the amiloride-sensitive sodium channel. *Nature* **389**, 607–610
43. Martin, C. E., and List, K. (2019) Cell surface-anchored serine proteases in cancer progression and metastasis. *Cancer Metastasis Rev.* **38**, 357–387
44. Scholz, C. C., Rodriguez, J., Pickel, C., Burr, S., Fabrizio, J. A., Nolan, K. A., *et al.* (2016) FIH regulates cellular metabolism through Hydroxylation of the deubiquitinase OTUB1. *PLoS Biol.* **14**, e1002347
45. Zhu, D., Xu, R., Huang, X., Tang, Z., Tian, Y., Zhang, J., *et al.* (2021) Deubiquitinating enzyme OTUB1 promotes cancer cell immunosuppression via preventing ER-associated degradation of immune checkpoint protein PD-L1. *Cell Death Differ.* **28**, 1773–1789
46. Liu, Y., Peng, K., Xie, R., Zheng, J., Guo, J., Wei, R., *et al.* (2019) Protocadherin gamma-A7 is down-regulated in colorectal cancer and associated with the prognosis in patients with wild-type KRAS. *Hum. Pathol.* **83**, 14–21
47. Abasi, M., Bazi, Z., Mohammadi-Yeganeh, S., Soleimani, M., Haghpanah, V., Zargami, N., *et al.* (2016) 7SK small nuclear RNA transcription level down-regulates in human tumors and stem cells. *Med. Oncol.* **33**, 128
48. Shen, C., Chai, W., Han, J., Zhang, Z., Liu, X., Yang, S., *et al.* (2023) Identification and validation of a dysregulated TME-related gene signature for predicting prognosis, and immunological properties in bladder cancer. *Front. Immunol.* **14**, 1213947
49. Uchimura, K., and Kitamura, K. (2015) [Prostasin (PRSS8) as a new pathological factor]. *Nihon Rinsho* **73**, 523–533
50. Bao, Y., Wang, Q., Guo, Y., Chen, Z., Li, K., Yang, Y., *et al.* (2016) PRSS8 methylation and its significance in esophageal squamous cell carcinoma. *Oncotarget* **7**, 28540–28555
51. Bao, Y., Li, K., Guo, Y., Wang, Q., Li, Z., Yang, Y., *et al.* (2016) Tumor suppressor PRSS8 targets Sphk1/S1P/Stat3/Akt signaling in colorectal cancer. *Oncotarget* **7**, 26780–26792

52. Desai, M. A., Webb, H. D., Sinanan, L. M., Scarsdale, J. N., Walavalkar, N. M., Ginder, G. D., *et al.* (2015) An intrinsically disordered region of methyl-CpG binding domain protein 2 (MBD2) recruits the histone deacetylase core of the NuRD complex. *Nucleic Acids Res.* **43**, 3100–3113
53. Zhang, L., Jia, G., Shi, B., Ge, G., Duan, H., and Yang, Y. (2016) PRSS8 is downregulated and suppresses Tumour growth and Metastases in hepatocellular carcinoma. *Cell. Physiol. Biochem.* **40**, 757–769
54. Bao, Y., Guo, Y., Yang, Y., Wei, X., Zhang, S., Zhang, Y., *et al.* (2019) PRSS8 suppresses colorectal carcinogenesis and metastasis. *Oncogene* **38**, 497–517
55. Ma, C., Ma, W., Zhou, N., Chen, N., An, L., and Zhang, Y. (2017) Protease serine S1 family member 8 (PRSS8) inhibits tumor growth in vitro and in vivo in human non-small cell lung cancer. *Oncol. Res.* **25**, 781–787
56. Yang, H. Y., Fang, D. Z., Ding, L. S., Hui, X. B., and Liu, D. (2017) Overexpression of protease serine 8 inhibits Glioma cell proliferation, migration, and invasion via suppressing the Akt/mTOR signaling pathway. *Oncol. Res.* **25**, 923–930
57. Cai, C., Zhang, Y., and Peng, X. (2021) Knocking down Sterol regulatory element binding protein 2 (SREBF2) inhibits the Serine Protease 8 (PRSS8)/sodium channel epithelial 1alpha subunit (SCNN1A) axis to reduce the cell proliferation, migration and epithelial-mesenchymal transformation of ovarian cancer. *Bioengineered* **12**, 9390–9400
58. Essigke, D., Bohnert, B. N., Janessa, A., Worn, M., Omage, K., Kalbacher, H., *et al.* (2022) Sodium retention in nephrotic syndrome is independent of the activation of the membrane-anchored serine protease prostasin (CAP1/PRSS8) and its enzymatic activity. *Pflugers Arch.* **474**, 613–624
59. Mendonsa, A. M., Na, T. Y., and Gumbiner, B. M. (2018) E-cadherin in contact inhibition and cancer. *Oncogene* **37**, 4769–4780
60. Loh, C. Y., Chai, J. Y., Tang, T. F., Wong, W. F., Sethi, G., Shanmugam, M. K., *et al.* (2019) The E-cadherin and N-cadherin Switch in epithelial-to-mesenchymal transition: signaling, therapeutic Implications, and challenges. *Cells* **8**, 1118
61. Conacci-Sorrell, M., Zhurinsky, J., and Ben-Ze'ev, A. (2002) The cadherin-catenin adhesion system in signaling and cancer. *J. Clin. Invest.* **109**, 987–991
62. Luke, J. J., Bao, R., Sweis, R. F., Spranger, S., and Gajewski, T. F. (2019) WNT/beta-catenin pathway activation Correlates with immune Exclusion across human cancers. *Clin. Cancer Res.* **25**, 3074–3083
63. Wang, J. Y., and Lu, A. Q. (2021) The biological function of m6A reader YTHDF2 and its role in human disease. *Cancer Cell Int.* **21**, 109
64. Chen, Z., Shao, Y. L., Wang, L. L., Lin, J., Zhang, J. B., Ding, Y., *et al.* (2021) YTHDF2 is a potential target of AML1/ETO-HIF1alpha loop-mediated cell proliferation in t(8;21) AML. *Oncogene* **40**, 3786–3798
65. Sanderson, M. R., Fahlman, R. P., and Wevrick, R. (2021) The N-terminal domain of the Schaaf-Yang syndrome protein MAGEL2 likely has a role in RNA metabolism. *J. Biol. Chem.* **297**, 100959
66. Hou, G., Zhao, X., Li, L., Yang, Q., Liu, X., Huang, C., *et al.* (2021) SUMOylation of YTHDF2 promotes mRNA degradation and cancer progression by increasing its binding affinity with m6A-modified mRNAs. *Nucleic Acids Res.* **49**, 2859–2877
67. Yang, Y., Yan, Y., Yin, J., Tang, N., Wang, K., Huang, L., *et al.* (2023) O-GlcNAcylation of YTHDF2 promotes HBV-related hepatocellular carcinoma progression in an N(6)-methyladenosine-dependent manner. *Signal Transduct. Target. Ther.* **8**, 63
68. Fang, R., Chen, X., Zhang, S., Shi, H., Ye, Y., Shi, H., *et al.* (2021) EGFR/SRC/ERK-stabilized YTHDF2 promotes cholesterol dysregulation and invasive growth of glioblastoma. *Nat. Commun.* **12**, 177
69. Yang, Z., Li, J., Feng, G., Gao, S., Wang, Y., Zhang, S., *et al.* (2017) MicroRNA-145 modulates N(6)-methyladenosine levels by targeting the 3'-Untranslated mRNA region of the N(6)-methyladenosine binding YTH domain family 2 protein. *J. Biol. Chem.* **292**, 3614–3623
70. Zhou, Y., Wu, J., Fu, X., Du, W., Zhou, L., Meng, X., *et al.* (2014) OTUB1 promotes metastasis and serves as a marker of poor prognosis in colorectal cancer. *Mol. Cancer* **13**, 258
71. Peters, D. E., Szabo, R., Friis, S., Shylo, N. A., Uzzun Sales, K., Holmbeck, K., *et al.* (2014) The membrane-anchored serine protease prostasin (CAP1/PRSS8) supports epidermal development and postnatal homeostasis independent of its enzymatic activity. *J. Biol. Chem.* **289**, 14740–14749
72. Szabo, R., Lantsman, T., Peters, D. E., and Bugge, T. H. (2016) Delineation of proteolytic and non-proteolytic functions of the membrane-anchored serine protease prostasin. *Development* **143**, 2818–2828
73. Friis, S., Madsen, D. H., and Bugge, T. H. (2016) Distinct developmental functions of prostasin (CAP1/PRSS8) Zymogen and activated prostasin. *J. Biol. Chem.* **291**, 2577–2582
74. Chen, L. M., Verity, N. J., and Chai, K. X. (2009) Loss of prostasin (PRSS8) in human bladder transitional cell carcinoma cell lines is associated with epithelial-mesenchymal transition (EMT). *BMC Cancer* **9**, 377
75. Chen, L. M., and Chai, K. X. (2002) Prostasin serine protease inhibits breast cancer invasiveness and is transcriptionally regulated by promoter DNA methylation. *Int. J. Cancer* **97**, 323–329
76. Chen, L. M., Hodge, G. B., Guarda, L. A., Welch, J. L., Greenberg, N. M., and Chai, K. X. (2001) Down-regulation of prostasin serine protease: a potential invasion suppressor in prostate cancer. *Prostate* **48**, 93–103
77. Takahashi, S., Suzuki, S., Inaguma, S., Ikeda, Y., Cho, Y. M., Hayashi, N., *et al.* (2003) Down-regulated expression of prostasin in high-grade or hormone-refractory human prostate cancers. *Prostate* **54**, 187–193
78. Valenta, T., Hausmann, G., and Basler, K. (2012) The many faces and functions of beta-catenin. *EMBO J.* **31**, 2714–2736
79. Liu, J., Xiao, Q., Xiao, J., Niu, C., Li, Y., Zhang, X., *et al.* (2022) Wnt/beta-catenin signalling: function, biological mechanisms, and therapeutic opportunities. *Signal Transduct. Target. Ther.* **7**, 3
80. Yeh, Y., Guo, Q., Connelly, Z., Cheng, S., Yang, S., Prieto-Dominguez, N., *et al.* (2019) Wnt/Beta-catenin signaling and prostate cancer therapy resistance. *Adv. Exp. Med. Biol.* **1210**, 351–378
81. Francis, J. C., Thomsen, M. K., Taketo, M. M., and Swain, A. (2013) beta-catenin is required for prostate development and cooperates with Pten loss to drive invasive carcinoma. *PLoS Genet.* **9**, e1003180
82. Wang, C., Chen, Q., and Xu, H. (2021) Wnt/beta-catenin signal transduction pathway in prostate cancer and associated drug resistance. *Discov. Oncol.* **12**, 40
83. Kaplan, Z., Zielske, S. P., Ibrahim, K. G., and Cackowski, F. C. (2021) Wnt and beta-catenin signaling in the Bone metastasis of prostate cancer. *Life (Basel)* **11**, 1099
84. Zhang, H., Liu, C., Zhu, D., Zhang, Q., and Li, J. (2023) Medicinal Chemistry Strategies for the development of inhibitors disrupting beta-Catenin's interactions with its nuclear partners. *J. Med. Chem.* **66**, 1–31
85. Song, T., Zou, Q., Yan, Y., Lv, S., Li, N., Zhao, X., *et al.* (2021) DOT1L O-GlcNAcylation promotes its protein stability and MLL-fusion leukemia cell proliferation. *Cell Rep.* **36**, 109739
86. Lv, S., Zhao, X., Zhang, E., Yan, Y., Ma, X., Li, N., *et al.* (2022) Lysine demethylase KDM1A promotes cell growth via FKBP8-BCL2 axis in hepatocellular carcinoma. *J. Biol. Chem.* **298**, 102374
87. Ruijter, J. M., Ramakers, C., Hoogaars, W. M., Karlen, Y., Bakker, O., van den Hoff, M. J., *et al.* (2009) Amplification efficiency: linking baseline and bias in the analysis of quantitative PCR data. *Nucleic Acids Res.* **37**, e45
88. Liu, J., Eckert, M. A., Harada, B. T., Liu, S. M., Lu, Z., Yu, K., *et al.* (2018) m(6)A mRNA methylation regulates AKT activity to promote the proliferation and tumorigenicity of endometrial cancer. *Nat. Cell Biol.* **20**, 1074–1083
89. Li, Z., Weng, H., Su, R., Weng, X., Zuo, Z., Li, C., *et al.* (2017) FTO plays an oncogenic role in Acute Myeloid leukemia as a N(6)-methyladenosine RNA demethylase. *Cancer Cell* **31**, 127–141
90. Song, T., Lv, S., Ma, X., Zhao, X., Fan, L., Zou, Q., *et al.* (2023) TRIM28 represses renal cell carcinoma cell proliferation by inhibiting TFE3/KDM6A-regulated autophagy. *J. Biol. Chem.* **299**, 104621